Copyright Warning & Restrictions

The copyright law of the United States (Title 17, United States Code) governs the making of photocopies or other reproductions of copyrighted material.

Under certain conditions specified in the law, libraries and archives are authorized to furnish a photocopy or other reproduction. One of these specified conditions is that the photocopy or reproduction is not to be "used for any purpose other than private study, scholarship, or research." If a, user makes a request for, or later uses, a photocopy or reproduction for purposes in excess of "fair use" that user may be liable for copyright infringement,

This institution reserves the right to refuse to accept a copying order if, in its judgment, fulfillment of the order would involve violation of copyright law.

Please Note: The author retains the copyright while the New Jersey Institute of Technology reserves the right to distribute this thesis or dissertation

Printing note: If you do not wish to print this page, then select "Pages from: first page # to: last page #" on the print dialog screen

ABSTRACT

POWER DISSIPATION AND MIXING TIME IN A PARTIALLY FILLED PHARMACEUTICAL REACTOR EQUIPPED WITH A RETREAT-BLADE IMPELLER AT DIFFERENT FILL RATIOS

by
Aniruddha Banerjee

Glass-lined, stirred reactors and tanks are of significant industrial importance, especially in the pharmaceutical and fine chemical industries. These reactors are manufactured with a "glass-lining," i.e., a glass layer applied to the agitator, the inside of the reactor/tank and to any of the surfaces in contact with its contents in order to maximize corrosion resistance, facilitate reactor cleaning, and minimize product contamination. Because of glass-lining fabrication issues, a retreat blade impeller with a low impeller clearance off the tank bottom is commonly used in glass-lined reactors. In addition, since wall baffles cannot be easily mounted on the wall of glass-lining reactors, a single baffle, such as a "beavertail" baffle, mounted from the top of the reactor is utilized instead.

Despite its common use in the pharmaceutical industry, some of the most important mixing characteristics of this type of reactor have not been fully studied, such as the power dissipated by the impeller under different baffling conditions and blend time, i.e., the time required by a system to achieve a predetermined level of homogeneity. Therefore, this work was focused on the determination of the impeller power dissipation and the blend time in these reactors as a function of a number of variables commonly varied during the operation of these reactors, including different liquid levels (fill ratios), impeller agitation speed, and baffling configurations.

In this study, a torispherical-bottomed, 61-L, scaled-down model of a commercial reactor (DeDietrich) similar to the type of glass-lined reactors frequently utilized in the pharmaceutical industry is used. The blend time and impeller power dissipation for this system are experimentally obtained as a function of liquid level (i.e., liquid height-to-tank diameter ratio, H/T), baffling configurations, and the agitation rates. Three baffling configurations are considered, i.e., a partially baffled system (where a single beavertail was used), a fully baffled system (i.e., four rectangular baffles) and an unbaffled system. The H/T ratio, corresponding to the ratio of the liquid level to the reactor diameter, is varied between 0.3 and 1. Six different agitation rates between 75 and 200 rpm are considered.

The Power Number, N_p, is found to be a function of the liquid level, baffling system, impeller type and impeller Reynolds Number. Larger values of N_p are associated with more completely baffled systems. In addition, N_p decreased with decreasing H/T ratios.

The blend time to achieve 95% homogeneity of a tracer, θ_{95}, is found to be inversely proportional to the agitation rate for the partially and fully baffled systems, although large deviations are present at lower H/T ratios. The blend time is not always inversely proportional to the agitation rate for the unbaffled system. The dimensionless blending time, $\theta_{95}N$, is also obtained for all baffling configurations, H/T ratios and agitation rates. $\theta_{95}N$ is found to be largely independent of the impeller Reynolds Number for the partially and fully baffled systems for H/T ratio between 0.7 and 1. The blend time and dimensionless blending time results indicate that they both are functions of the liquid level, impeller Reynolds Number and baffling configuration.

POWER DISSIPATION AND MIXING TIME IN A PARTIALLY FILLED PHARMACEUTICAL REACTOR EQUIPPED WITH A RETREAT-BLADE IMPELLER AT DIFFERENT FILL RATIOS

by
Aniruddha Banerjee

A Thesis
Submitted to the Faculty of
New Jersey Institute of Technology
in Partial Fulfillment of the Requirements for the Degree of
Master of Science in Chemical Engineering

Otto H. York Department of
Chemical, Biological and Pharmaceutical Engineering

May 2013

APPROVAL PAGE

POWER DISSIPATION AND MIXING TIME IN A PARTIALLY FILLED PHARMACEUTICAL REACTOR EQUIPPED WITH A RETREAT-BLADE IMPELLER AT DIFFERENT FILL RATIOS

Aniruddha Banerjee

Dr. Piero M. Armenante, Thesis Advisor Date
Distinguished Professor of Chemical, Biological and Pharmaceutical Engineering, NJIT

Dr. Laurent Simon, Committee Member Date
Associate Professor of Chemical, Biological and Pharmaceutical Engineering, NJIT

Dr. Robert B. Barat, Committee Member Date
Professor of Chemical, Biological and Pharmaceutical Engineering, NJIT

Biographical Sketch

Author: Aniruddha Banerjee

Degree: Master of Science

Date: May 2013

Undergraduate and Graduate Education:

- Master of Science in Chemical Engineering
  New Jersey Institute of Technology, Newark, NJ, 2013

- Bachelor of Science in Chemical Engineering
  New Jersey Institute of Technology, Newark, NJ, 2011

Major: Chemical Engineering

Learn from yesterday, live for today, hope for tomorrow. The important thing is not to stop questioning.

Albert Einstein

ACKNOWLEDGMENT

I would like to express my deepest gratitude to Dr. Piero Armenante, my advisor, for not only giving me the opportunity to work with him, but also for contributing his expertise and insights during the course of my research. I would also like to give my sincerest appreciation to Dr. Laurent Simon and Dr. Robert B. Barat for consenting to take part in my committee.

Furthermore, I would like to give a special thanks to Nonjaros Chomcharn who lent me his prior research experience in this field and Magnus Jeran for his support in my work. For the constant support and encouragement that was given to me by my family, especially my parents, that motivated me to not only finish my thesis and academic career, but also be a success in all of my endeavors: Thank you.

TABLE OF CONTENTS

TABLE OF CONTENTS
(Continued)

LIST OF TABLES

LIST OF FIGURES

LIST OF FIGURES
(Continued)

List of Symbols

D	Diameter of the impeller (mm)
H	Liquid level (mm)
T	Diameter of the tank (mm)
C	Clearance of the impeller from the bottom of the tank (mm)
Re	Impeller Reynolds Number
N	Agitation Rate (rpm)
μ	Dynamic liquid viscosity (Pa·s)
ρ	Liquid density (kg/m^3)
N_P	Power Number
Γ	Torque (N·m)
P	Power (W)
I	Green light intensity
$\bar{I}$	Normalized green light intensity
θ_D	Mixing time to reach a particular uniformity level (s)
θ_{95}	Mixing time to reach a 95% uniformity level (s)

CHAPTER 1

INTRODUCTION

1.1 Background

Glass-lined, stirred reactors are of immense importance specifically in the pharmaceutical industry among others. Glass lining (the term lining is used to refer to the glass coating on the agitator and the inside of the tank) provides corrosion resistance, is easy to clean, and eliminates product contamination [3]. Glass-lined reactors often utilize a retreat blade impeller with a low impeller clearance from the bottom of the tank. The retreat blade impeller with rounded blade corners may limit harmful turbulence effects while maintaining circulation throughout the vessel [3]. However, it is required to manufacture the vessel without pre-attached baffles due to the presence of the glass lining. Usually a single baffle is utilized, i.e. typically a beavertail baffle, which is mounted from the top of the reactor. Without the presence of baffles or with insufficient baffling , the fluid moves in a swirling motion creating a central vortex leading to insufficient mixing [8]. Hence, the utilization of baffles eliminates the formation of the vortex and promotes a well-mixed system.

A standard baffling configuration consists of four vertical plates having width equal to 8 to 10% (T/12 to T/10) of the tank diameter [10] and mounted at the tank wall. There is a drawback with using wall baffles because cleaning is more difficult, unlike in an unbaffled tank. Since cleaning is very important in the pharmaceutical industry and critical in the manufacturing of pharmaceutical products, typically a beavertail baffle is preferred in glass-lined reactors. In recent years, improvements in mixing technology and glass formulations have led to new impeller designs, however, little has been published

about the performance characteristics of the mixing equipment, including Power Number data [3].

One factor that has a major role in the mixing performance of a system is the blending time, commonly known as the mixing time. Blending time is defined as the time taken to reach a predetermined degree of homogeneity [10]. Mixing time may depend on a variety of factors, such as where the materials to be mixed are added, the location of the impeller, and the time required before a fluid can be considered mixed [11]. The degree of mixing in a system is a function of two variables: the forces producing turbulence, i.e. the driving force, and the forces tending to dampen the formation of turbulence, i.e. the resistance [6].

The conductivity method and the colorimetric method are the two common methods used to determine the blending time. The conductivity method uses a probe to measure the local conductivity as a function of time when an electrolyte is added to the liquid system as the marker [10]. Although this technique is relatively simple, the insertion of the conductivity probe in the vessel can affect the flow dynamics in the system. The alternative is to utilize the colorimetric method which is a non-intrusive method. The colorimetric method utilizes the concept of color change in the presence of an indicator to measure the blending time. The blending time at a particular location can be measured using visual inspection or through image processing of digitized images of the mixing system. Image processing software detects the color evolution at particular locations on the image allowing the determination of a very precise blending time. It has been concluded in a separate work that the colorimetric method is highly reproducible and can identify unmixed zones [1].

1.2 Objectives

The objective of this work is focused on experimentally determining the blending time and the impeller power dissipation in a pharmaceutical vessel for different fill ratios, agitation rates, and baffling configurations. This research uses an exact scale-down model of a ~61 L De Dietrich reactor, a cylindrical reactor with a torispherical bottom, along with a retreat-blade impeller for all of the experiments. The De Dietrich reactor used here is similar to a glass-lined reactor that is frequently utilized in the pharmaceutical industries. The blending time and impeller power dissipation is dependent on three different variables: the baffling configurations, the liquid level, and the agitation rates. Three baffling configurations are considered: unbaffled, partially baffled (i.e. a single beavertail is used), and fully baffled (i.e. four rectangular baffles) systems. The H/T ratio, corresponding to the ratio of the liquid level to the reactor diameter, is varied between 0.3 and 1. Lastly, six different agitation rates between 75 and 200 rpm are considered. The non-intrusive, colorimetric method was utilized combined with digital imaging analysis for the blending time experiments.

CHAPTER 2

THEORETICAL BACKGROUND

2.1 Power Number

The power dissipated by an impeller in a mixing system is obtained by calculating the product of the torque, applied to the impeller, and the agitation rate:

$$P = 2\pi(N)\Gamma \tag{2.1}$$

The power can then be used to calculate the Power Number, N_P, which is a non-dimensional number. The Power Number is defined by Equation 2.2:

$$N_P = \frac{P}{\rho N^3 D^5} \tag{2.2}$$

where the power is divided by $\rho N^3 D^5$ to make the Power Number dimensionless. The power number depends on a number of dimensionless variables [10] and can be summarized as follows:

$$N_P = f\left(\frac{\rho N D^2}{\mu}, \text{baffle type, impeller type and geometry}, \frac{T}{D}, \frac{H}{T}, \frac{C}{D}, \ldots\right) \tag{2.3}$$

It can be seen from Equation 2.2 that N_P is dependent on the impeller Reynolds Number:

$$Re = \frac{\rho N D^2}{\mu} \tag{2.4}$$

Furthermore, N_P is also a function of the baffle type, impeller type and geometry and various geometric ratios including the tank diameter-to-impeller diameter ratio, the liquid level-to-tank diameter ratio, the impeller clearance-to-impeller diameter ratio, etc.

For a given system geometry where the flow is in a turbulent regime and the Reynolds Number is high, i.e. typically $Re > 10^4$, the Power Number is only a function of

$$N_P = f\left(\text{baffle type}, \text{impeller type and geometry}, \frac{T}{D}, \frac{H}{T}, \frac{C}{D}, \ldots\right) \quad (2.5)$$

Therefore, the Power Number varies depending on the type of the impeller and baffling configuration used and, more importantly, on the H/T ratio.

2.2 Blending Time and Dimensionless Blending Time

Similar to the Power Number, the blending time, θ_D, is also a function of the impeller Reynolds Number, baffling configuration, impeller type, the liquid level-to-tank diameter ratio, H/T, impeller clearance-to-impeller diameter ratio, and other such ratios. For a given system geometry and impeller type, θ_D is simply dependent on the Reynolds Number, H/T and the baffling configuration.

A literature review suggests that the dimensionless blending time, $\theta_D N$, in *baffled systems* is a constant and independent of Reynolds Number [10]. However, the variation in the H/T ratio and baffling configuration needs to be considered when all other variables are defined. This also means that $\theta_D N$ can no longer be considered independent of the Reynolds Number. Thus, $\theta_D N$ becomes:

$$\theta_D N = f\left(\frac{\rho N D^2}{\mu}, \text{baffle type}, \frac{H}{T}\right) \quad (2.6)$$

Although $\theta_D N$ is a function of the Reynolds Number, H/T, and baffling configuration, Equation 2.6 becomes a constant when considering only a *single* H/T ratio in ***baffled systems***. When considering a 95% blending time in ***baffled systems*** and a *single* H/T ratio, $\theta_D N$ becomes:

$$\theta_{95} N = \text{Constant} \quad (2.7)$$

However, information on the behavior of the dimensionless blending time in a partially and unbaffled system is not available. Ergo, Equation 2.6 should be utilized when looking at the dimensionless blending time in such systems.

CHAPTER 3

EXPERIMENTAL SYSTEM AND METHOD

3.1 Mixing Apparatus

An open cylindrical tank with a torisheprical bottom was utilized as the mixing tank for the entirety of this research. This mixing vessel was commissioned and paid for by Eli Lilly (thanks to Dr. Billy Allen, Eli Lilly, Indianapolis, IN). The tank was fabricated, specifically for this research, with the assistance of Dr. David Brown through the BHR Group based in the UK. The tank is made up of a thin (0.5 mm) fluorinated ethylene propylene co-polymer (FEP) rigid film that has a refractive index of 1.338, i.e., very similar to that of water (1.333). This ensures the minimization of any curvature effects during the image digitizing and processing steps. The vessel has an internal diameter, *T,* of 450 mm and an overall height of 540 mm. The overall height includes the cylindrical and torispherical bottom sections measuring at 430 mm and 110 mm, respectively.

There is a rigid collar and lip at the top of the tank allowing it to be suspended in a larger "host" tank, i.e., a square tank was used, as shown in Figure 3.1. During each experiment, the mixing vessel was placed in a square Plexiglas tank and both vessels were filled with water. The “host” tank was filled up to a height similar to that of the mixing vessel in order to eliminate any differential pressure existing between the two tanks, which otherwise would have caused the mixing vessel to rupture.

3.2 Agitation System

A single retreat three-blade curved impeller, typically used with glass-lined vessels in the pharmaceutical industry, was used in all of the experiments. The following are the impeller dimensions measured with a caliper: impeller diameter (D) = 203 mm; the radius of curvature of the blades = 92.08 mm; height of the blade = 25.4 mm; thickness of the blade = 12.7 mm; and an impeller diameter-to-tank diameter ratio, D/T, of 0.451. The impeller clearance off the tank bottom, C, was maintained at 100 mm for all the experiments. The corresponding impeller clearance-to-tank diameter ratio (C/T) is 0.222. The impeller was donated by Dr. San Kiang of Bristol-Myers Squibb, New Brunswick, NJ.

This scaled-down impeller is based on a model designed and manufactured by the De Dietrich Company, a leading manufacturer of glass-lined equipment and accessories for the pharmaceutical and chemical industries. The impeller was attached to the end of a shaft that has a diameter of 12.52 mm and is located centrally inside the tank. The impeller, coupled to an inline transducer (described below), was connected to a 1/4- HP motor (Chemglass, Model CG-2033-11) controlled by an external controller (Chemglass, Model CG-2033-31).

For the purpose of conducting test runs for power dissipation experiments, the retreat blade (mentioned above) and a rushton impeller was used. The rushton impeller that is used has a diameter of 126.8 mm, disk diameter of 84.5 mm, disk thickness of 2.6 mm, blade width of 32 mm, blade length of 25 mm, and a blade thickness of 28 mm [7]. *Only* for the test runs, three locations are considered for both the impellers, i.e. impeller clearance, C, of 100 mm (C_1), 170 mm (C_2), and 200 mm (C_3).

3.3 Baffles

The tank was operated under three different baffling configurations, i.e., unbaffled, partially baffled, and fully baffled. A single beavertail baffle, shown in Figure 3.1 (b), was used for the partially baffled system. The beavertail baffle has the following dimensions: diameter of the top section = 15.24 mm; length of the top section = 70.64 mm; diameter of the middle section = 22.23 mm; length of the middle section = 199.7 mm; diameter of the bottom section = 20.07 mm; length of the bottom section = 70.64 mm. The baffle clearance was kept constant at 170 mm from the bottom of the mixing tank. The baffle was placed midway between the center of the tank and the vessel wall.

The fully baffled system, shown in Figure 3.1 (C), consists of four vertical metal plates which are mounted from the top of the vessel. Four acrylic rectangular plates were attached to each of the metal plates for the purpose of increasing the baffle width. The total width of the baffle was 45 mm and the clearance was the same as in the case of the beavertail baffle.

(a) 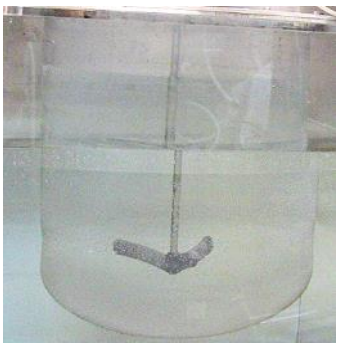 (b) 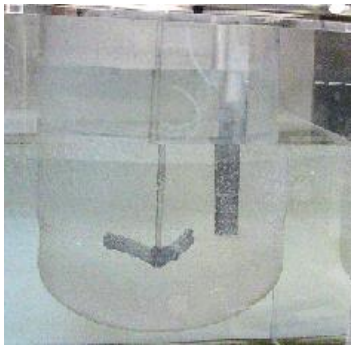 (c) 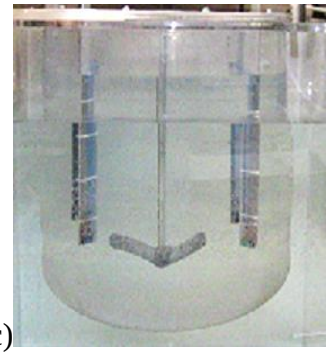

Figure 3.1 Mixing System:
(a) Unbaffled tank
(b) Partially baffled tank with a beavertail baffle
(c) Fully baffled tank

3.4 Materials

The external rectangular tank and the mixing tank, shown in Figure 3.1, are both filled with tap water for the purpose of power measurements. For the blending time experiments, the rectangular tank is filled with tap water while deionized water is used in the mixing tank. Additionally, a Phenolphthalein indicator, 12 mol/L HCl (Fisher Scientific) and 97% reagent grade of NaOH beads (Sigma-Aldrich) are used in the blending time experiments. A digital video camera (VIXIA HF200 NTSC, Canon) is also used for filming the blending time experiments.

3.5 Experimental Procedure for the Determination of Power Dissipation

The torque (Γ) which is applied to the impeller by the 1/4- HP motor was experimentally measured using a strain gage-based rotary torque transducer (Model, T6-5-Dual Range, Interface, Inc. Scottsdale, AZ). The transducer is connected to the Interface series 9850 Multi-Channel Load Cell Indicator. The transducer can measure the torque in two different scales, i.e., 0-0.5 Nm and 0-5 Nm. Only the first scale is used in this work. The same instrument could also measure the agitation speed, N, and internally calculate the instantaneous power delivered, P, by the shaft according to Equation 2.1.

The indicator utilized the M700 software to interface with a computer, which was used for data acquisition and processing. Before collecting the power data, the system was allowed to stabilize for 3 minutes. After a steady state was reached, power data was collected for 3 minutes and each experiment is conducted in triplets. Equation 2.2 is used to obtain the experimental Power Number, N_P.

3.6 Experimental Procedure for the Determination of Blending Time

The blending time is experimentally determined using the colorimetric method. The colorimetric method is a technique that is based on the change in color of an indicator during an acid-base reaction. A Phenolphthalein indicator, which is pink when the pH > 10 (color of a basic solution) and colorless when the pH < 8 (color of an acidic solution), is used. The reaction between HCl (strong acid) and NaOH (strong base) is utilized. Before the start of each experiment, 10 mL of a 10 mol/L NaOH solution is added to the deionized water in the mixing tank. This increased the pH of the deionized water from an initial approximate pH of 5 to an approximate pH of 11. The addition of the base resulted in a pink solution due to the presence of the phenolphthalein indicator. At the beginning of each experiment, 10 mL of a 12 mol/L HCl solution is rapidly added at the air-liquid interface and adjacent to the shaft.

A digital video camera (VIXIA HF200 NTSC, Canon) is used to capture the color evolution from pink to colorless at a rate of 29 frames/s. A white sheet of paper was placed around the rectangular vessel to obtain a homogenous illumination. The video in MTS format is then converted to an AVI format using the ApecSoft M2TS to AVI MP4 DVD Converter 1.8.0. The AVI formatted video is then analyzed with MATLAB to extract the green component of the light intensity. The green component of the light intensity is analyzed on each image at eleven fixed "sampling" locations as shown in Figure 3.2. At each sampling point, the intensity of the green color component, I, is extracted from each image and normalized using Equation 3.4, where I_{in} and I_f are the initial and final green light intensity, respectively. The normalized intensity, $\bar{I}$, is then

plotted as a function of time for each experiment in order to determine the mixing time θ_{95}.

$$\bar{I} = \frac{I(t) - I_{in}}{I_f - I_{in}} \tag{3.4}$$

This research utilizes the 95% blending time, θ_{95}, which is defined as the time required for the normalized intensity, in Equation 3.4, to reach and always remain within the 95%-105% interval of the final equilibrium value. It is important to note that there is no special significance in using the 95% of the final normalized intensity value as the time when equilibrium is achieved. 95% level of uniformity is simply a common endpoint to choose for blending processes where it can be assumed that the process has achieved equilibrium. However, other such levels of uniformity can also be considered such as 99%, 99.9%, or even 99.99% that correspond to θ_{99}, $\theta_{99.9}$, and $\theta_{99.9}$, respectively.

Each experiment is repeated three times and the resulting values are averaged. The largest mixing time out of the 11 sampling locations is taken as the 95% mixing time for the entire system. At the end of each repetition, the batch is neutralized by adding NaOH solution until the pH is approximately 11, as measured with a pH meter (HANNA Instruments HI 221 Calibration Check Microprocessor pH Meter). Reusing the batch for all three repetitions reduces the consumption of deionized water.

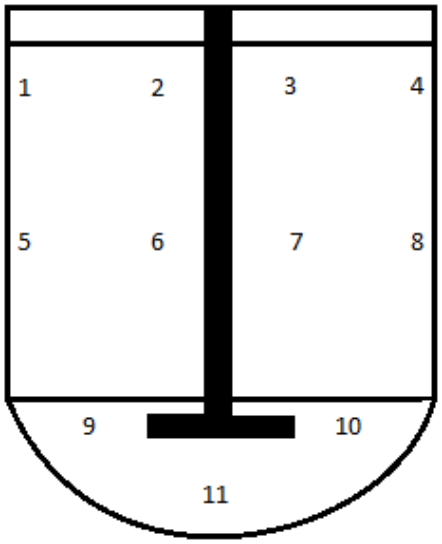

Figure 3.2 11 sampling points analyzed in MATLAB for the colorimetric method.

3.7 Data Analysis and Presentation

The rotational speed is varied between 75 rpm to 200 rpm in 25 rpm increments for both the power dissipation and blending time experiments. The liquid level-to-tank diameter ratio, H/T, is varied between 0.3 and 1 in increments of 0.1 for both power dissipation and blend time experiments. Table 3.1 and 3.2 shows the Reynolds Number for the various agitation rates and the liquid level and volume for the H/T ratios, respectively.

Table 3.1 Reynolds Number at Different Agitation Rates

Agitation Rate, N (RPM)	Reynolds Number, Re
75	51164
100	68219
125	85274
150	102329
175	119383
200	136438

Table 3.2 H/T Ratios with the Corresponding Liquid Level and Volume

H/T	Liquid Level, H (mm)	Liquid Volume (L)
0.3	135	13.50
0.4	180	18.59
0.5	225	25.75
0.6	270	32.90
0.7	315	40.06
0.8	360	47.21
0.9	405	54.37
1	450	61.53

An important note to make is that the H/T ratio of 0.3 is a completely unbaffled region, even when considering a partially or fully baffled system. Hence, the data for the impeller power dissipation and mixing experiments for the H/T ratio of 0.3 is only presented for the unbaffled system. For the impeller power dissipation experiments, the results will include the impeller Power Number for different baffling systems, fill ratios, and agitation rates along with N_P vs. Re plots. N_P vs. H/T plots will also be given. Supplemental Power Number data for a rushton and retreat blade impeller at different impeller clearances, C, will also be provided for the fully baffled system with an H/T ratio of 1.

Furthermore, the results for the mixing experiments will include the mixing time, θ_{95}, θ_{95} vs. N, and $\theta_{95}N$ vs. Re for different baffling systems, fill ratios, and agitation rates, where $\theta_{95}N$ is the dimensionless blending time. Additionally, θ_{95} vs. H/T, and $\theta_{95}N$ vs. H/T will also be presented.

CHAPTER 4

RESULTS

4.1 Retreat Blade Impeller Power Numbers for Different Baffling Configurations, Fill Ratios, and Agitation Rates

A Power Number vs. Reynolds Number plot of H/T of 1 for the retreat blade impeller is shown in Figure 4.1 and the corresponding Power Number data is given in Table 4.1 below. Figures 4.2-4.5 are the Power Number vs. Reynolds Number plot for the remaining H/T ratios. A comprehensive set of data is included in Appendix A.1. In each H/T ratio, there is a decrease in the Power Number for all three baffling configurations as the agitation rate is increased. This indicates that for a defined impeller type and geometry, the Power Number is a function of the baffling configuration, fill ratio and Reynolds Number. However, in theory the Power Number should be independent of the impeller Reynolds Number for Re > 10^4. An explanation is given in Chapter 5.1. Although there is a decreasing trend in all of the baffling systems, the unbaffled system has the steepest decreasing trend out of all the configurations. Furthermore, for the H/T ratio of 0.5 and 0.4, the partially baffled system also sees a large decreasing trend.

Table 4.1 Agitation Rates, Power Number, and Reynolds Number for the Retreat Blade Impeller for Different Baffling Configurations with H/T of 1

			Power Number, N_P		
H/T	**Agitation Rate, N (RPM)**	**Reynolds Number, Re**	**Unbaffled**	**Partially Baffled**	**Fully Baffled**
1	75	51164	0.355	0.601	0.838
	100	68219	0.297	0.547	0.763
	125	85278	0.277	0.541	0.759
	150	102329	0.266	0.555	0.757
	175	119383	0.262	0.540	0.742
	200	136438	0.295	0.520	0.724

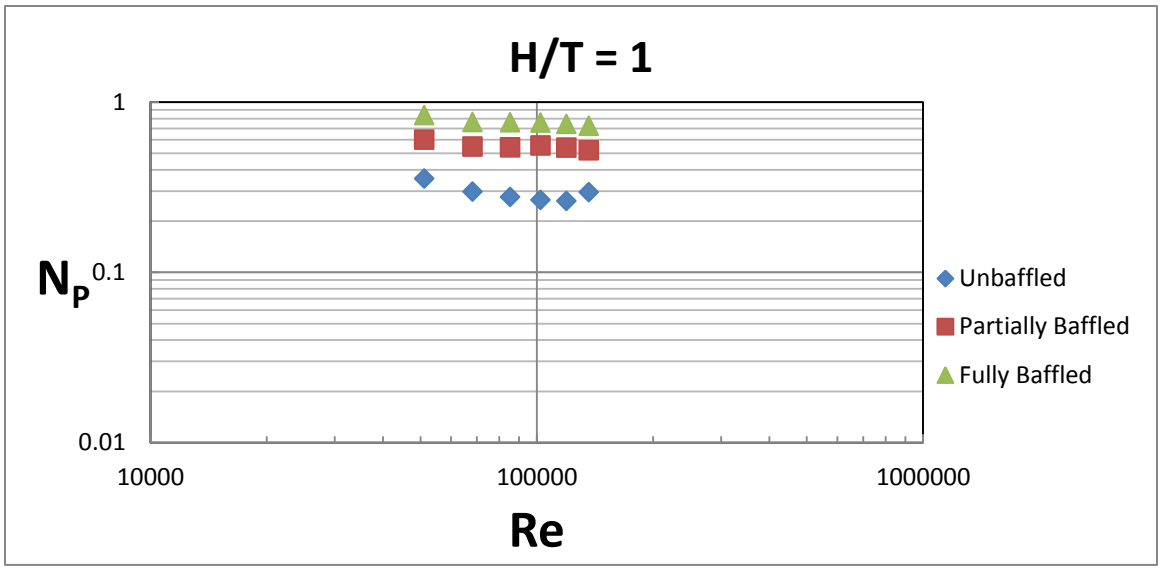

Figure 4.1 Power Number vs. Reynolds Number Plot for Different Baffling Configurations with H/T of 1.

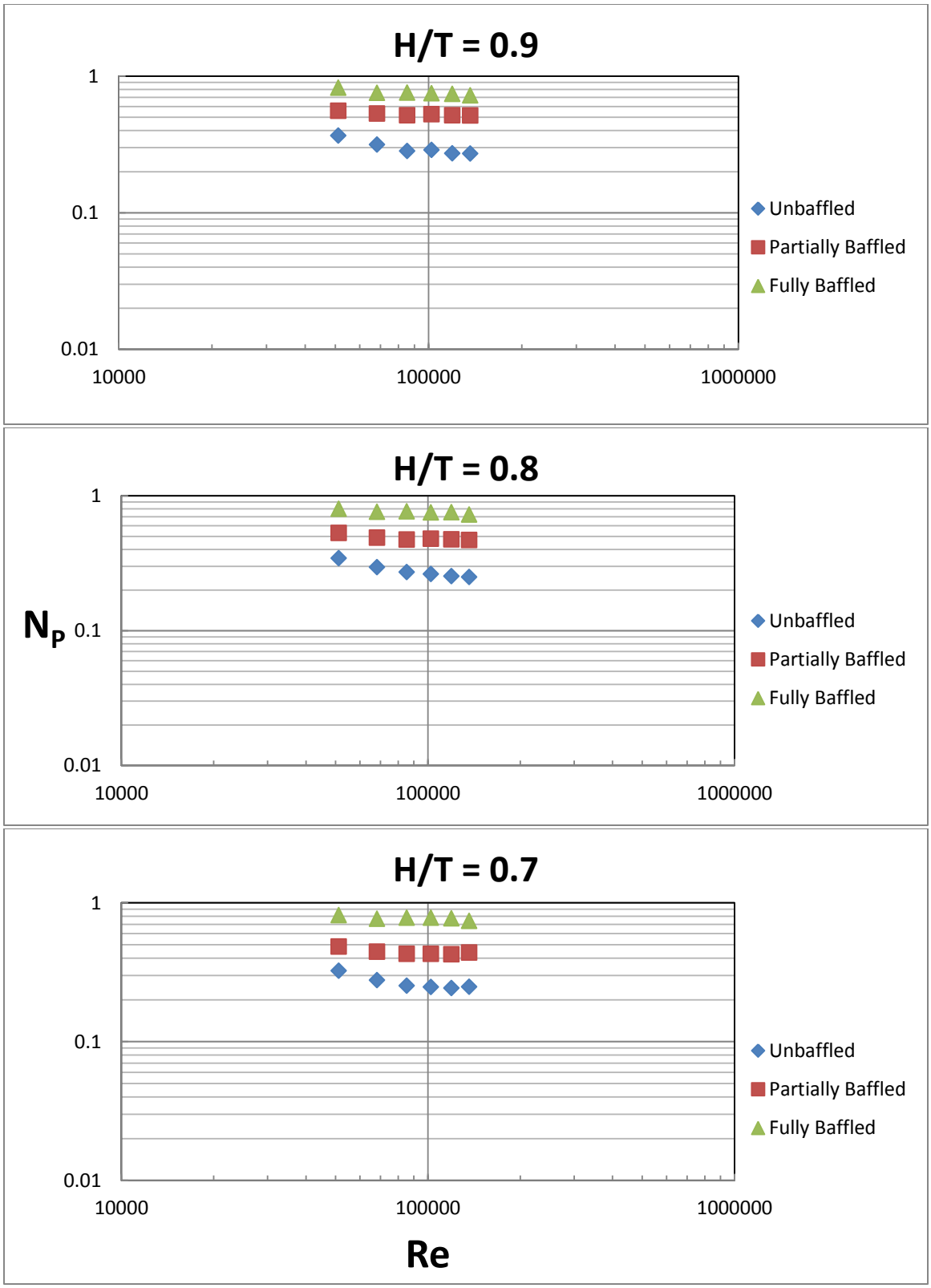

Figure 4.2 Power Number vs. Reynolds Number Plots for Different Baffling Configurations and H/T of 0.7-0.9.

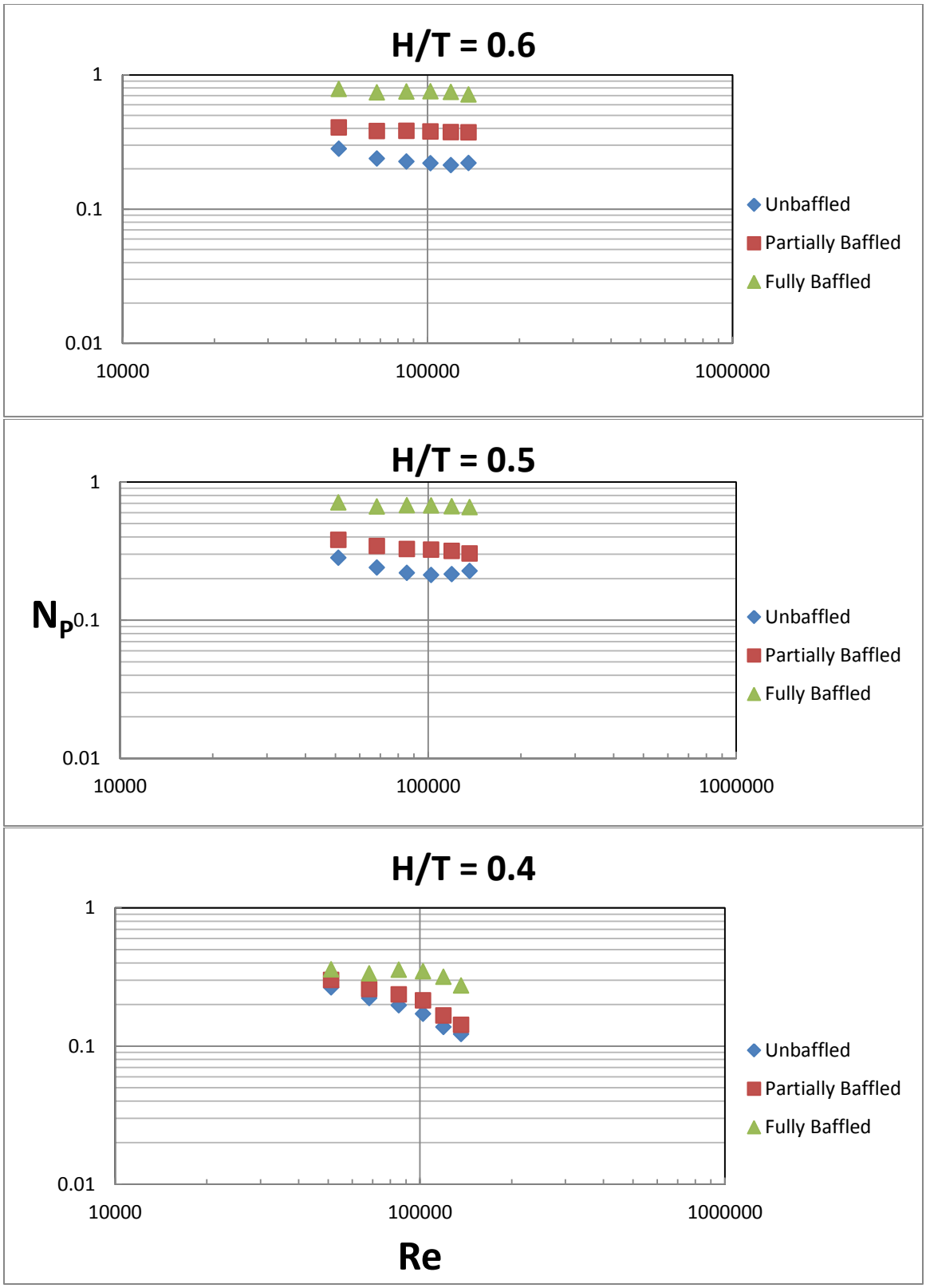

Figure 4.3 Power Number vs. Reynolds Number Plots for Different Baffling Configurations and H/T of 0.4-0.6.

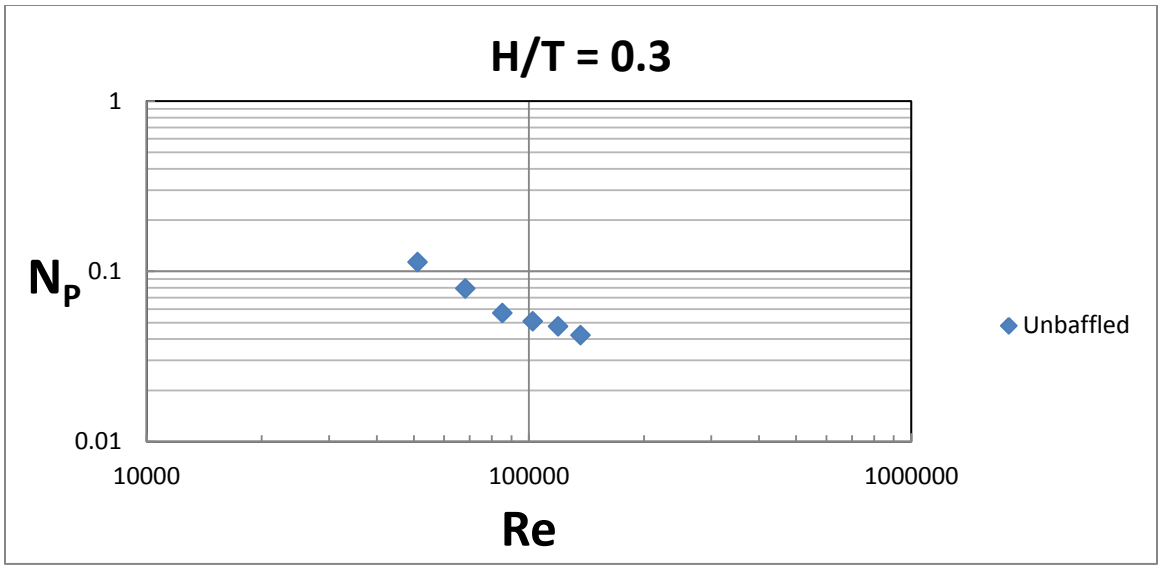

Figure 4.4 Power Number vs. Reynolds Number Plot for Different Baffling Configurations and an H/T of 0.3.

For a fully baffled system, the Power Number ranges from 0.838 to 0.275, with an overall decrease in the Power Number as the fill ratio, H/T, is decreased from 1 to 0.4. The Power Number in the partially baffled system has a range of 0.601 to 0.142 and sees the same trend as the fully baffled system when the fill ratio is decreased to 0.4. Similarly, the unbaffled system has the same decreasing trend in the Power Number as the fill ratio is lowered and has a range of 0.355 to 0.042. In all of the impeller power dissipation experiments, a vortex formation is observed. The size and depth of this vortex increased as the agitation rate is increased. Table A.5 in Appendix A.3 lists the agitation rate for vortex formation for each baffling configuration and fill ratio.

Figure 4.5 shows the Power Number vs. fill ratio plots for different baffling systems at specific agitation rates. It is clearly evident from Figure 4.5 that the Power Number varies for each baffling system and thus, is a function of the baffling configuration. Furthermore, as the fill ratio decreases the Power Number also decreases which means that the Power Number is also a function of the fill ratio.

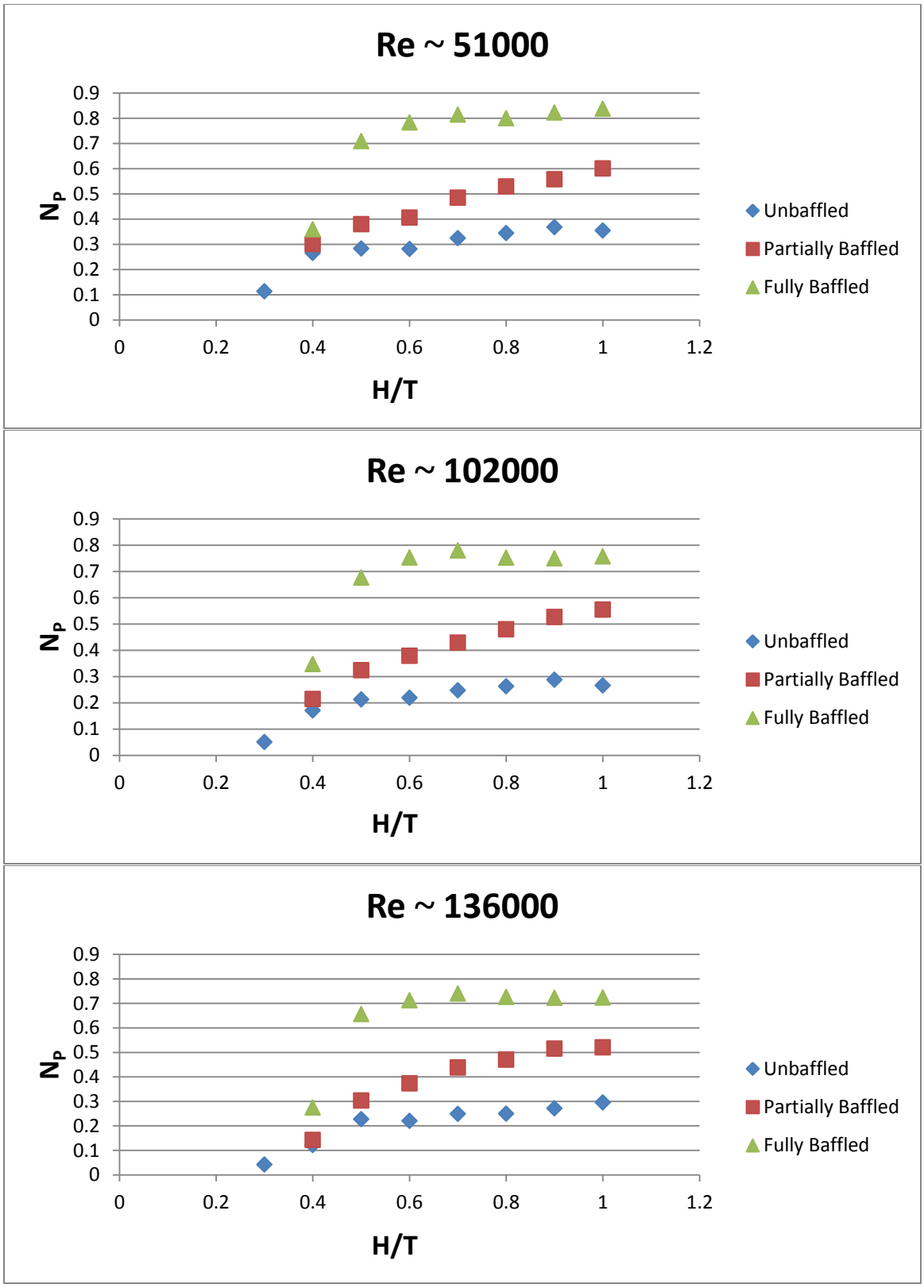

Figure 4.5 Power Number vs. Fill Ratio Plots at Specific Reynolds Number for all Baffling Configurations.

4.2 Retreat Blade and Rushton Impeller Power Numbers at Different Locations for a Fully Baffled System with H/T of 1

As mentioned earlier, supplemental power dissipation experiments is conducted using the retreat blade and rushton impellers. For only these sets of experiments, three locations are considered for both the impellers, i.e. impeller clearance, C, of 100 mm (C_1), 170 mm (C_2), and 200 mm (C_3). Both impellers are in a completely "unbaffled" environment for C_1, "partially baffled" environment for C_2 and in a "fully baffled" region for C_3.

Table 4.2 summarizes the Power Number data for both impellers at six agitation rates and Figure 4.6 has the corresponding Power Number vs. Reynolds Number plot. It can be seen from Table 4.2 that the Power Number for the retreat blade impeller has a decreasing trend, as observed earlier in Chapter 4.1, at all three locations. However, the same trend does not exist for the rushton impeller at each of these locations. The Power Number is fairly steady and deviates between 4.69 and 4.45 for C_1, 4.41 and 4.29 for C_2, and 5.01 and 4.75 for C_3. The result for the rushton impeller is consistent with Equation 2.5 presented in Chapter 2.1.

Table 4.2 Power Number Data for the Retreat Blade and Rushton Impellers at 3 Different Impeller Clearances for an H/T of 1

Agitation Rate, N (RPM)	**Retreat Blade Impeller Power Number**			**Rushton Impeller Power Number**		
	C_1	**C_2**	**C_3**	**C_1**	**C_2**	**C_3**
75	7.914	8.100	8.162	4.643	4.413	4.816
100	7.752	7.645	8.005	4.610	4.297	4.870
125	7.525	7.312	7.736	4.587	4.261	4.841
150	7.443	7.465	7.627	4.458	4.334	4.753
175	7.375	7.284	7.474	4.507	4.341	4.799
200	7.179	7.339	7.262	4.695	4.402	5.012

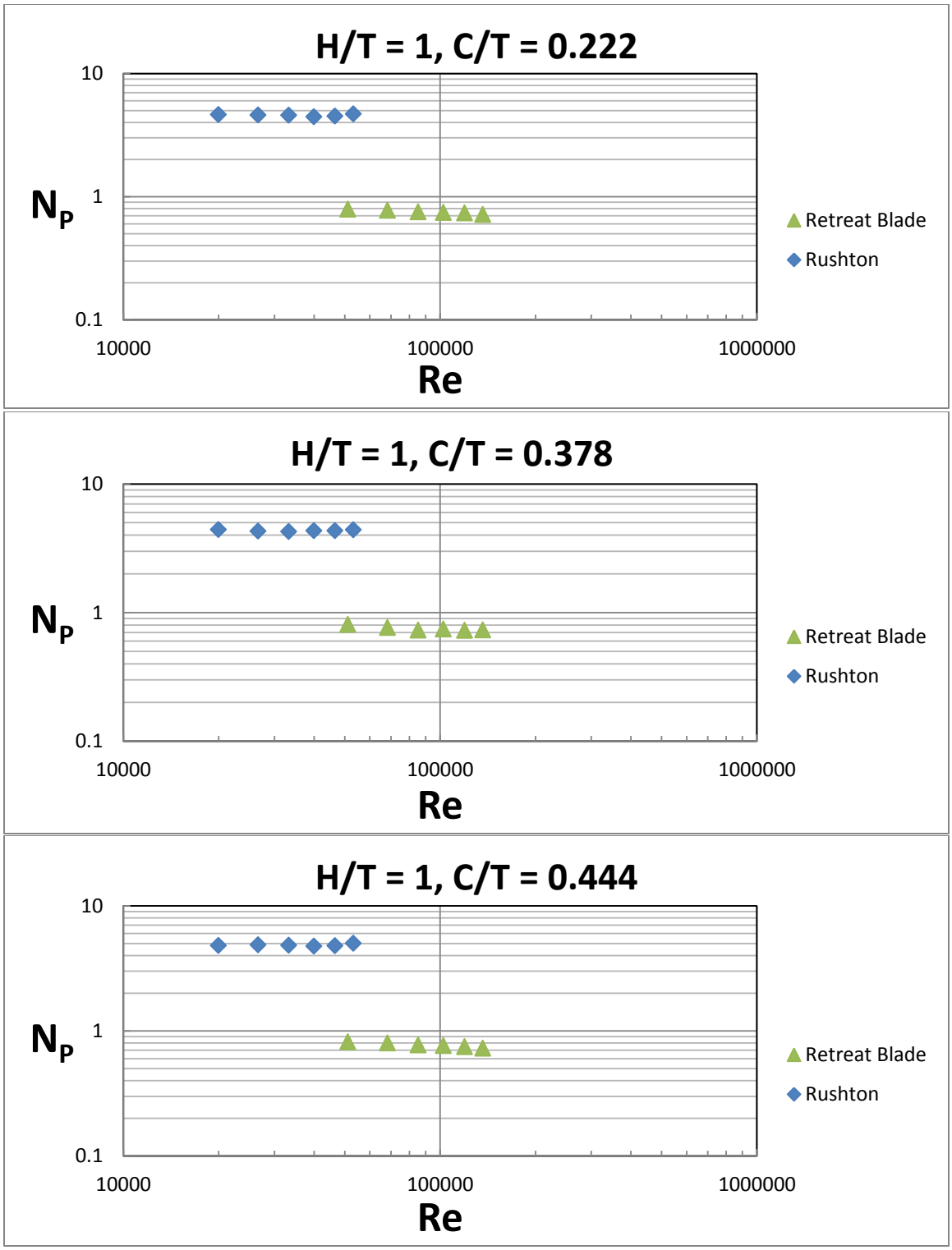

Figure 4.6 Power Number vs. Reynolds Number Plots for the Retreat Blade and Rushton Impellers at 3 Different Impeller Clearances for an H/T of 1.

4.3 Blending Time and Dimensionless Blending Time for Different Baffling Configurations, Fill Ratios, and Agitation Rates

Figures 4.7 and 4.8 shows the typical green light intensity output and the normalized intensity as a function of time at sampling location 7 (refer to Figure 3.2). Figures 4.7 and 4.8 presents the plots for the fully baffled system and an H/T ratio of 1 for 75 rpm. Figure 4.9a shows the blending time at each of the sampling locations in the mixing vessel for the fully baffled system at H/T of 1 and 75 rpm. Figure 4.9b shows the color evolution pattern in the mixing vessel as observed in all the blending time experiments. For all of the blending time experiments, a vortex is observed at specific agitation rates for all of the baffling configurations. The size and depth of this vortex increased as the agitation rate is increased. Table A.5 in Appendix A.3 lists the agitation rate for vortex formation at each baffling configuration and fill ratio.

The color evolution pattern presented in Figure 4.9b was visually observed during the course of each blending time experiment. The area below and around the impeller, Region 1, was the first to change in color from pink to colorless. Region 2 is where the next de-colorization occurred from around the Region 1-2 interface, moving up the vessel wall, and towards the surface. Region 3 is the last area to change in color. This evolution pattern has also been observed in [2].

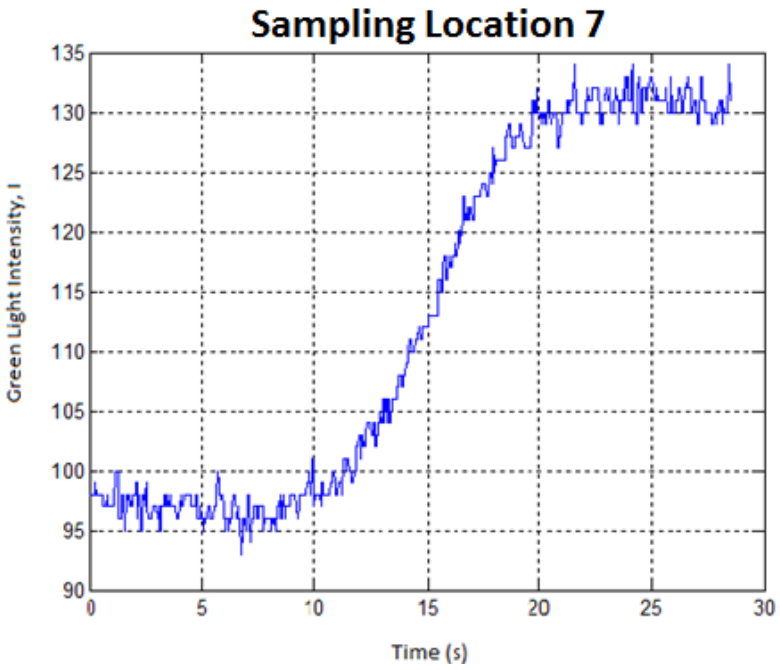

Figure 4.7 Green Light Intensity vs. Time at Sampling Location 7 for the Fully Baffled System and an H/T of 1.

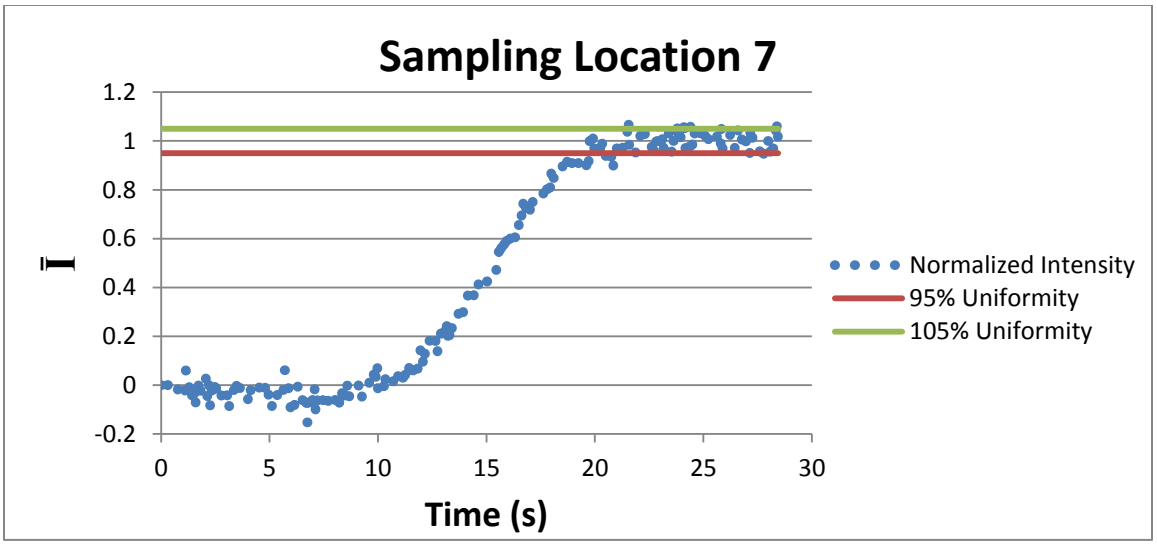

Figure 4.8 Normalized Intensity vs. Time at Sampling Location 7 for the Fully Baffled System and an H/T of 1.

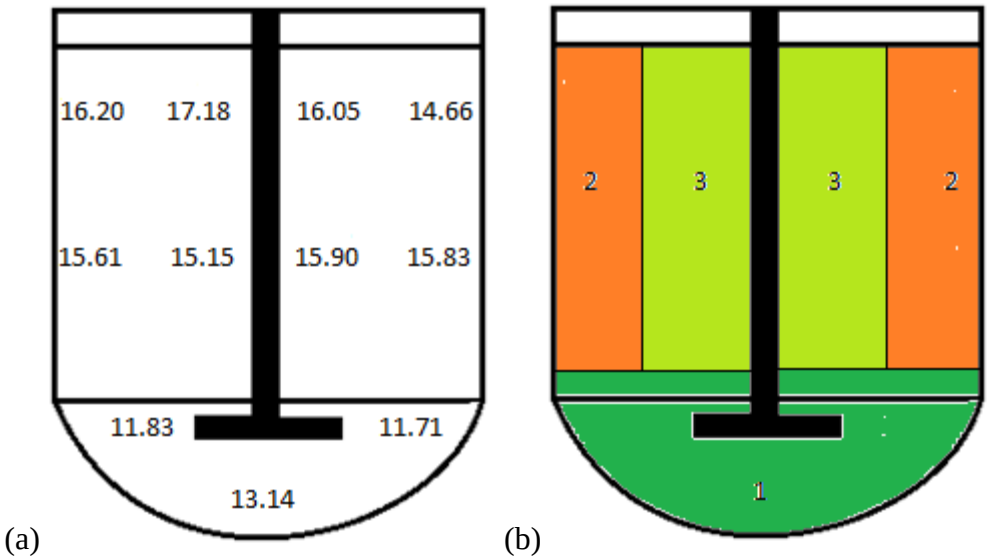

(a) (b)

Figure 4.9: (a) Blending Time at Individual Sampling Locations for a Fully Baffled System at an H/T of 1 and 75 RPM
(b) Color Evolution Pattern in the Vessel for all Experiments

The highest blending time, θ_{95}, for the fully baffled system with an H/T ratio of 1 is found to be 17.18 s at an agitation rate of 75 rpm, whereas the lowest time is 7.64 s for the 200 rpm agitation rate. Similarly, the highest blending time for the partially baffled system with an H/T ratio of 1 is found to be 33.82 s at an agitation rate of 75 rpm and the lowest time is 9.82 s for the 200 rpm agitation rate. However, there is a marked increase in the blending time for the unbaffled system where the highest time is found to be 432.33 s at 75 rpm and the lowest time is 43.48 s at *175 rpm*, not at 200 rpm. The results indicate that θ_{95} is indeed a function of the baffling configuration and agitation rate for a *particular* H/T ratio, as was discussed in Chapter 2.2.

The dimensionless blending time, $\theta_{95}N$, for the fully baffled system is fairly constant and ranges between 21.48 and 25.47 for an H/T of 1. This verifies Equation 2.7 in Chapter 2.2 where $\theta_{95}N$ is a constant for baffled systems at a particular H/T ratio. The dimensionless blending time for the partially baffled system is between 22-23 for the 75-

100 rpm range, 45-47 for the 125-175 rpm range, and 32.73 at 200 rpm. However, for the unbaffled system, the dimensionless blending time has a wide range between 126 and 540, as in the similar case for blending time. The blending time and dimensionless blending time results presented in Table 4.3 are for the three baffling configurations with an H/T of 1 and for 75-200 rpm. Figure 4.10 presents the plot for the blending time vs. agitation rate and the dimensionless blending time vs. Reynolds for an H/T of 1. Figures 4.11-4.13 and Figures 4.14-4.16 shows the plot for the blending time vs. agitation rate and the dimensionless blending time vs. Reynolds for the remaining H/T ratios, respectively.

Table 4.3 Blending Time and Dimensionless Blending Time for Different Baffling Configurations, Agitation Rates, and H/T of 1

H/T	**1**		
	Unbaffled	**Partially Baffled**	**Fully Baffled**
Agitation Rate, N (RPM)		**θ_{95} (s)**	
75	432.33	33.82	17.18
100	161.01	25.72	13.56
125	171.33	22.76	10.89
150	162.14	18.89	9.47
175	43.48	15.75	8.73
200	49.64	9.82	7.64
Agitation Rate, N (RPM)		**θ_{95}N**	
75	540.41	42.28	21.48
100	268.35	42.87	22.60
125	356.94	47.42	22.69
150	405.35	47.23	23.66
175	126.82	45.94	25.46
200	165.47	32.73	25.47

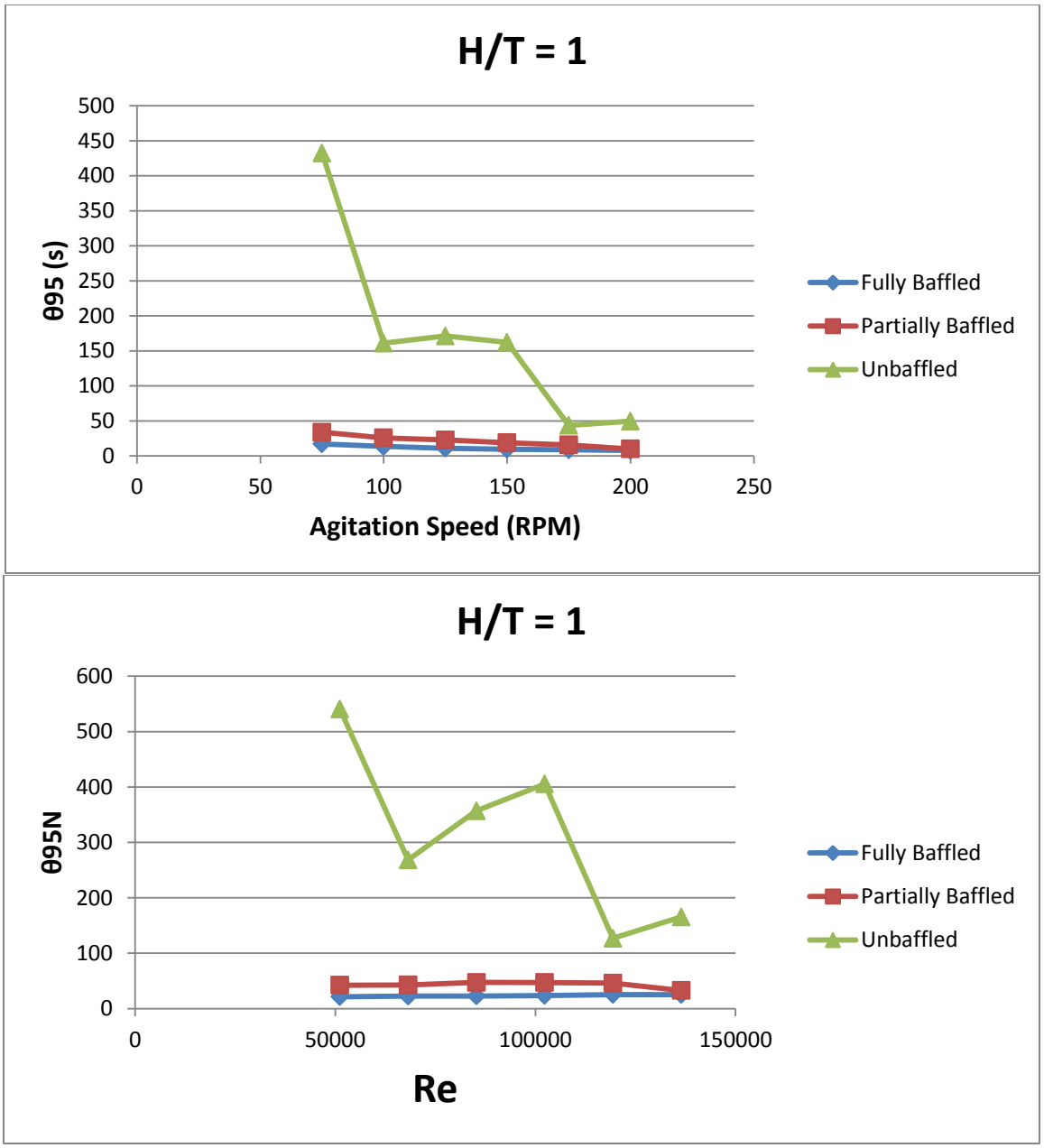

Figure 4.10 Blending Time vs. Agitation Rate and Dimensionless Blending Time vs. Reynolds Number Plots for Different Baffling Configurations and an H/T of 1.

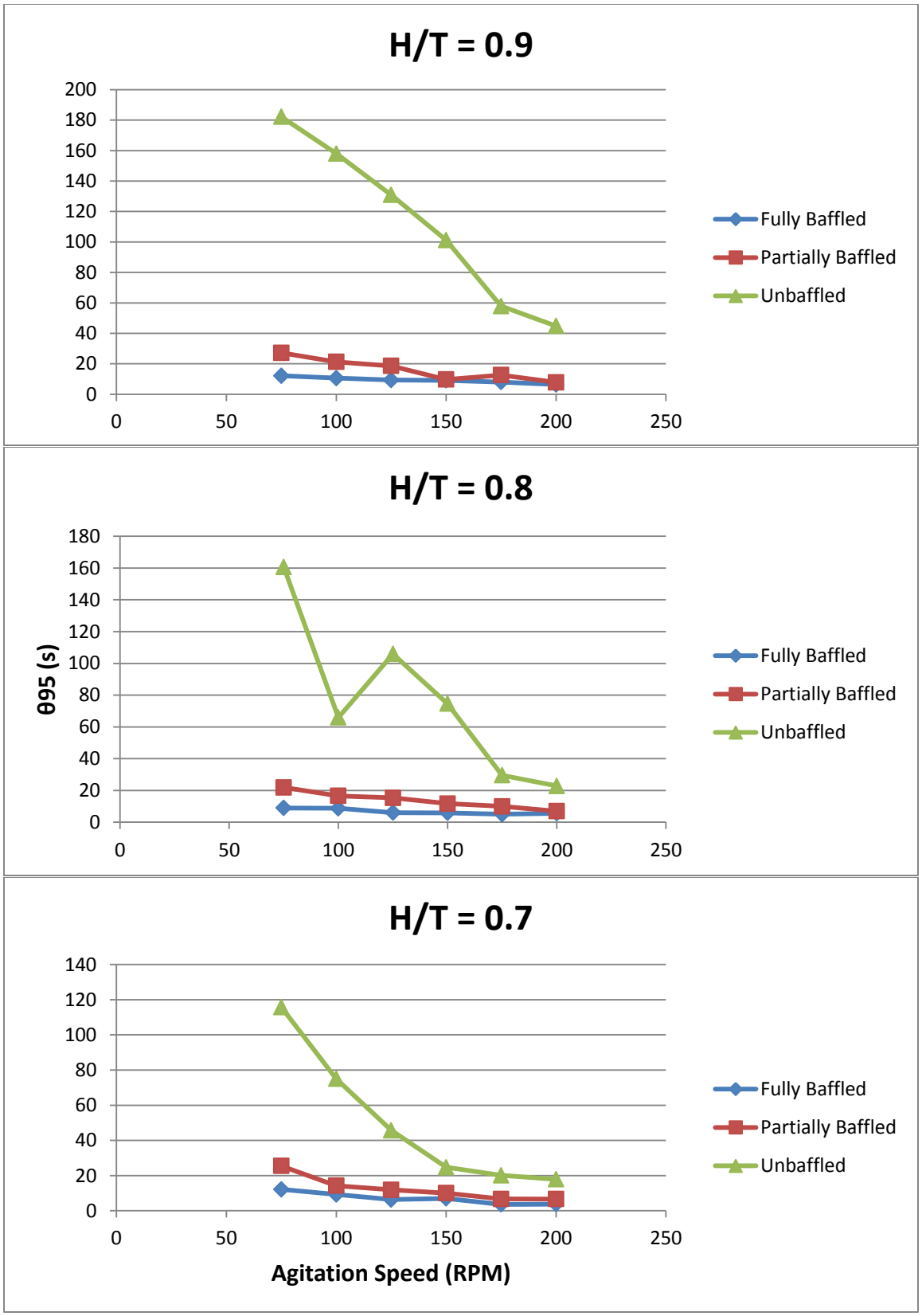

Figure 4.11 Blending Time vs. Agitation Rate Plots for Different Baffling Configurations and H/T of 0.7-0.9.

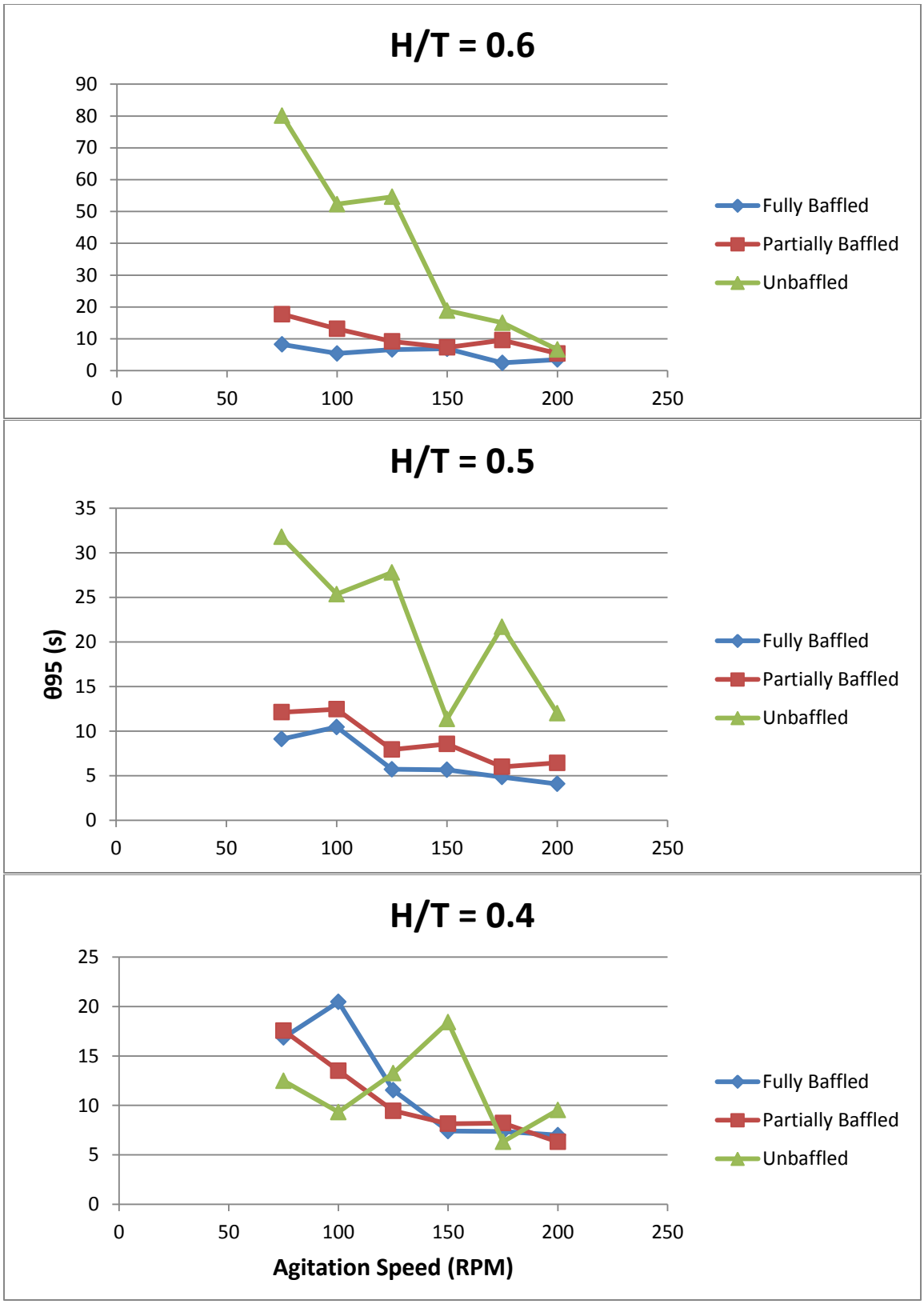

Figure 4.12 Blending Time vs. Agitation Rate Plots for Different Baffling Configurations and H/T of 0.4-0.6.

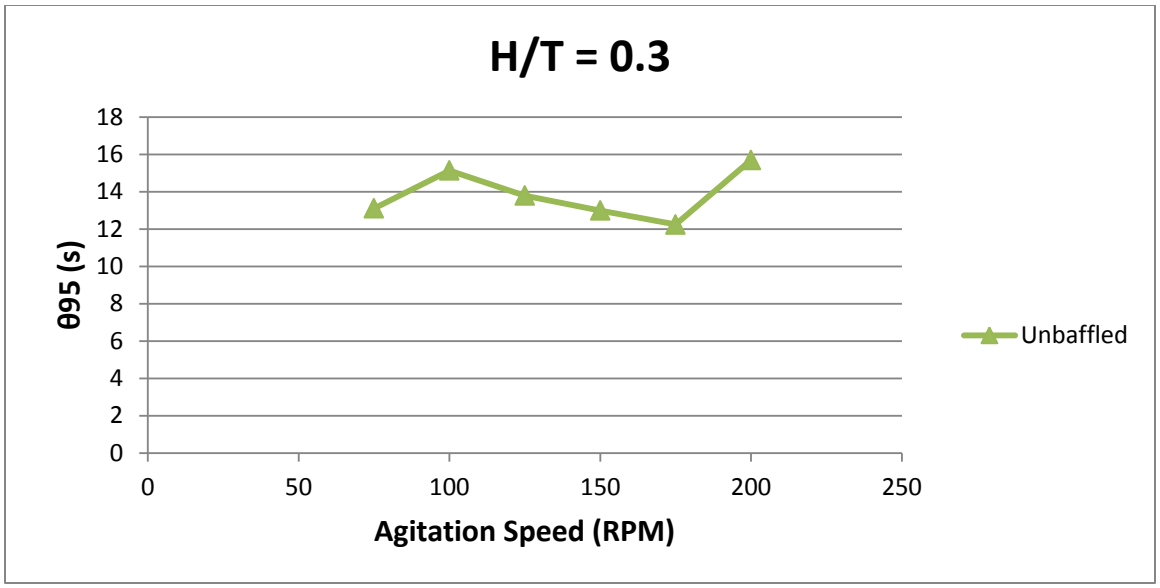

Figure 4.13 Blending Time vs. Agitation Rate Plot for Different Baffling Configurations and an H/T of 0.3.

Generally, the blending time is found to have a higher value in the unbaffled system and the time decreases as the system becomes better baffled. This trend holds true for decreasing H/T ratios and increasing agitation rates. However, the blending time for the H/T ratio of 0.3 does not have a particular trend.

From Figures 4.14-4.16, it can be seen that the dimensionless blending time is fairly constant between H/T of 0.7-1 for the partially and fully baffled systems. However, as the fill ratio is decreased, an erratic behavior is observed in both of these baffling systems. The unbaffled system, on the other hand, does not follow a specific trend. Clearly, it is evident that $\theta_{95}N$ is a function of the Reynolds Number and the baffling configuration. The complete set of data for the blending time and the dimensionless blending time at the varying fill ratios is included in Appendix A.2.

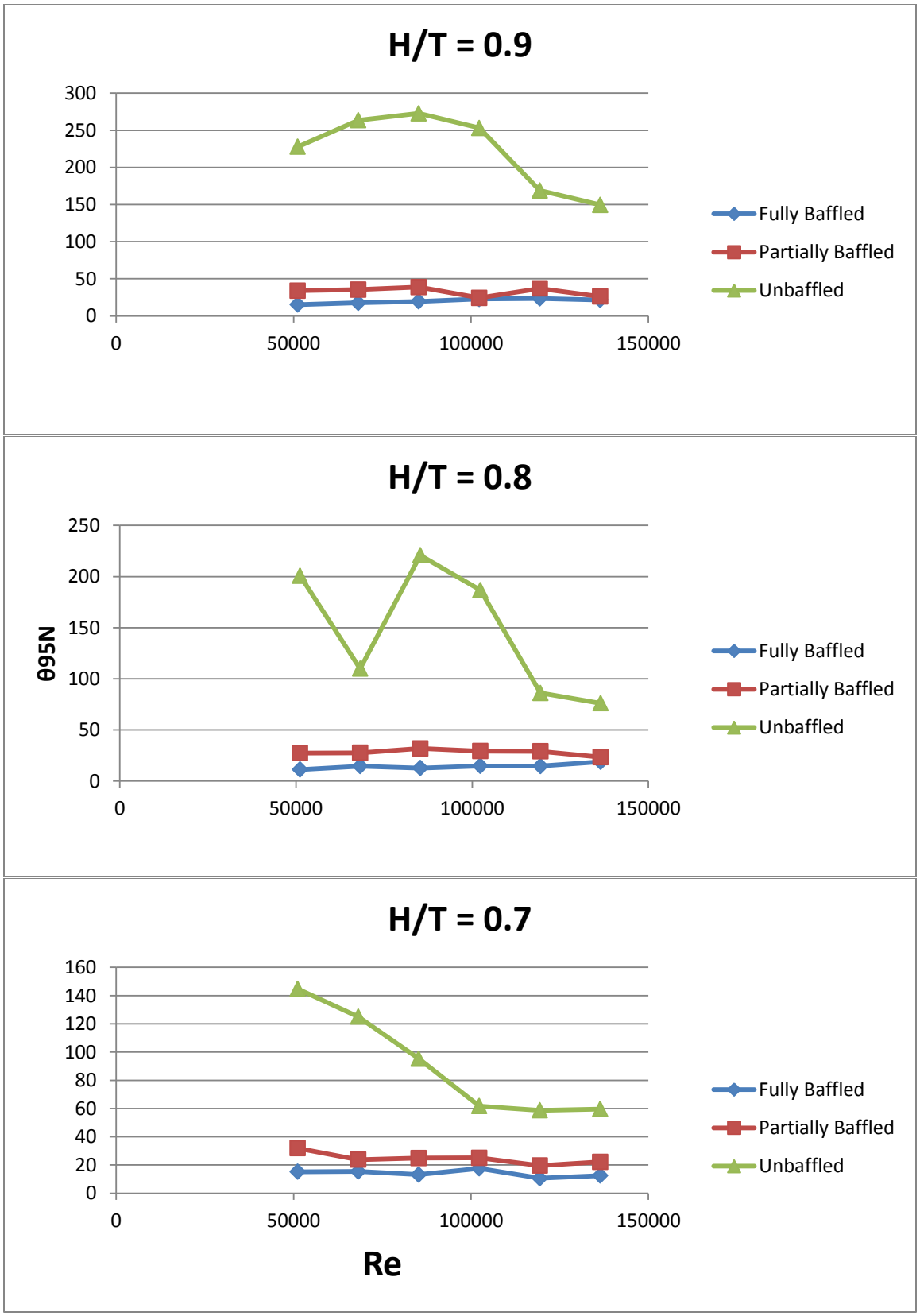

Figure 4.14 Dimensionless Blending Time vs. Reynolds Number Plots for Different Baffling Configurations and H/T of 0.7-0.9.

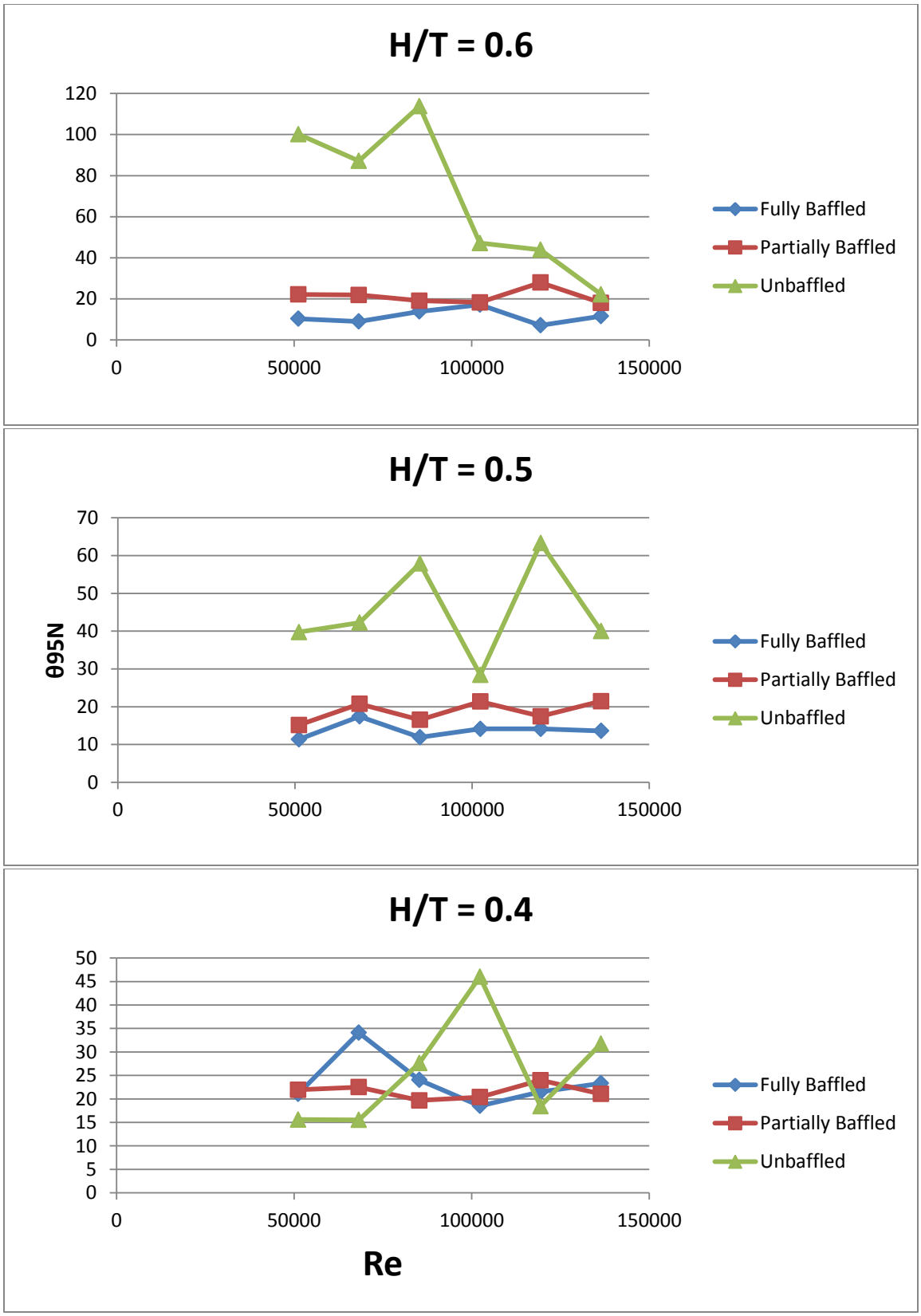

Figure 4.15 Dimensionless Blending Time vs. Reynolds Number Plots for Different Baffling Configurations and H/T of 0.4-0.6.

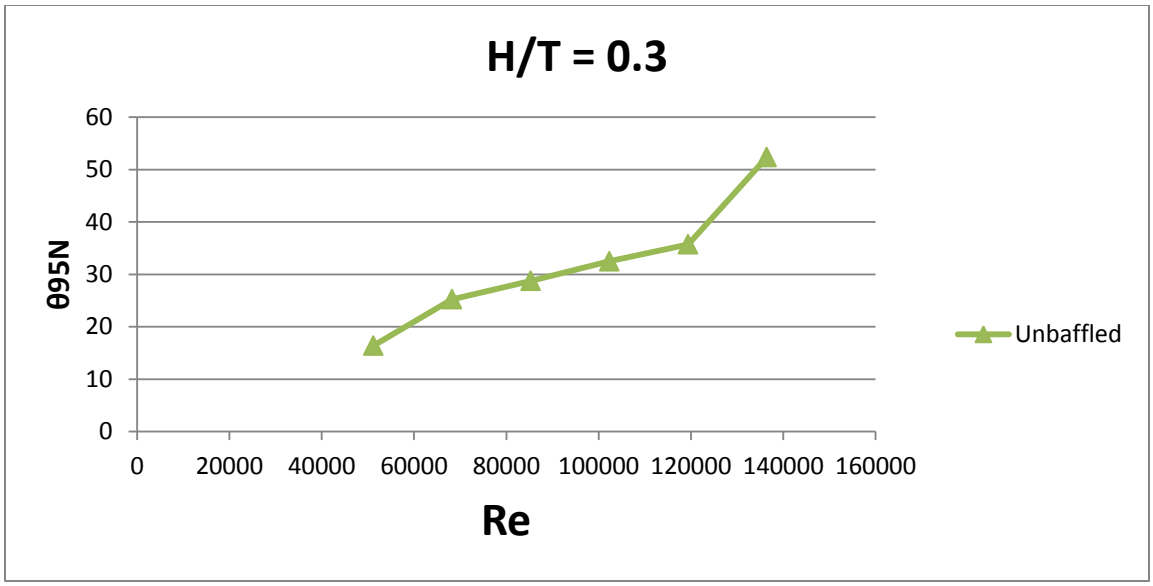

Figure 4.16 Dimensionless Blending Time vs. Reynolds Number Plots for Different Baffling Configurations and H/T of 0.3.

Figures 4.17-4.18 show the plots for the blending time and dimensionless blending time vs. the fill ratio for all baffling configurations at a specific agitation rate. Both figures reinforces the fact that θ_{95} and $\theta_{95}N$ are not only a function of baffling configuration, but also strongly dependent on the fill ratio, H/T, as was discussed in Chapter 2.2.

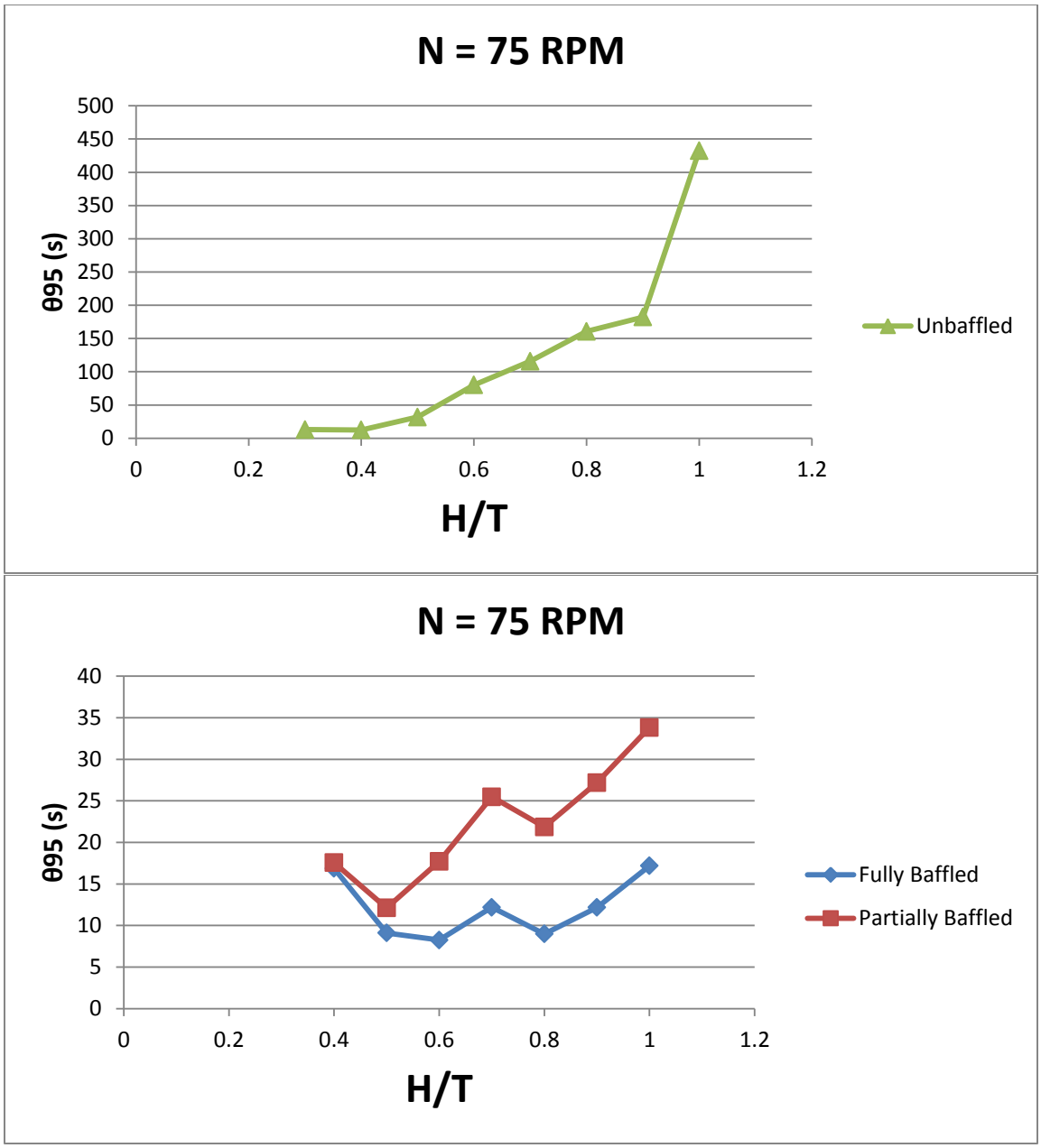

Figure 4.17 Blending Time vs. Fill Ratio Plots for Different Baffling Configurations and 75 RPM.

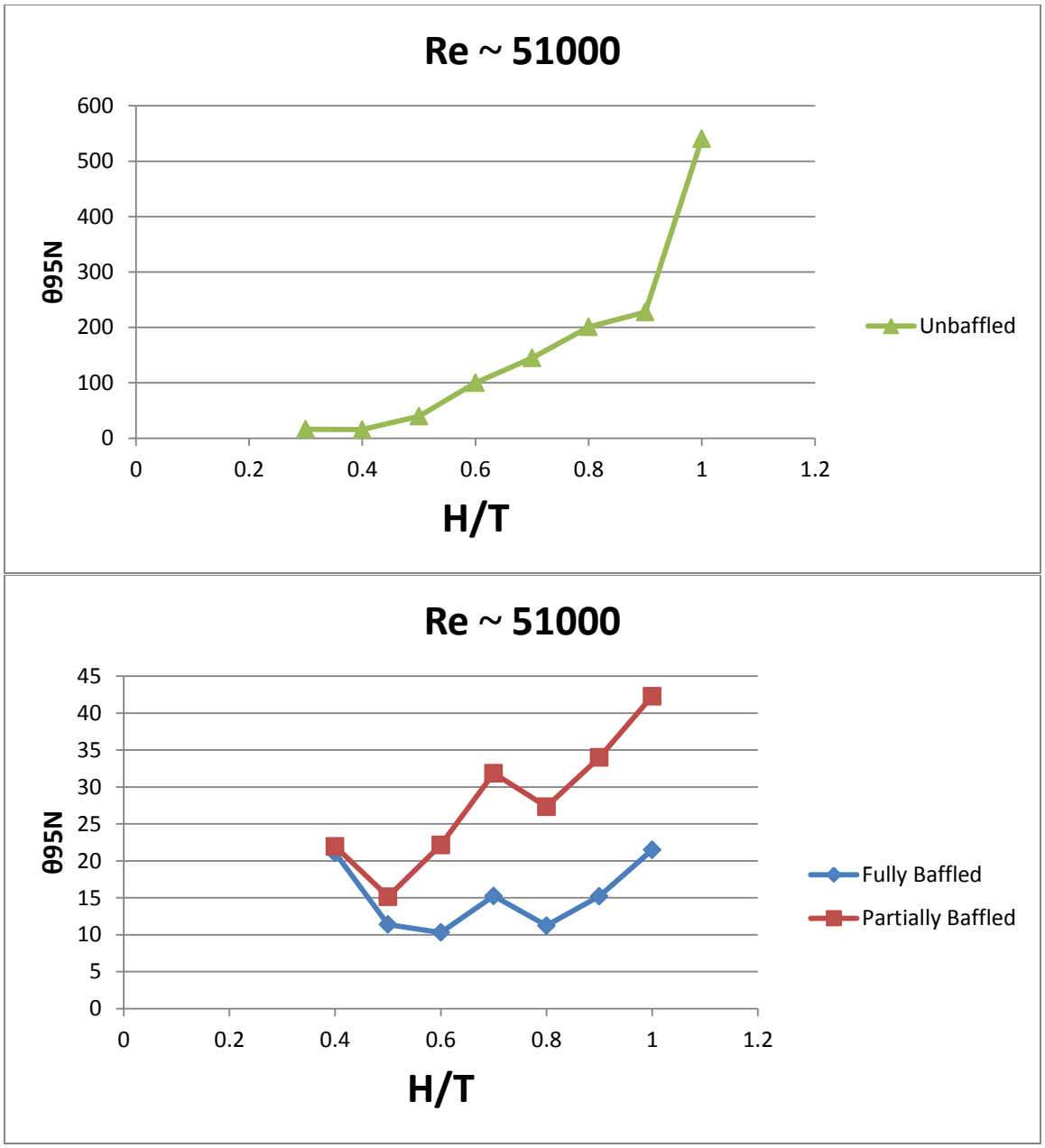

Figure 4.18 Dimensionless Blending Time vs. Fill Ratio Plots for Different Baffling Configurations and a Reynolds Number of 51000.

CHAPTER 5

DISCUSSION

5.1 Effect of the Torispherical Bottom on the Impeller Power Numbers

At high Reynolds Numbers, greater than about 10^4, the flow is *turbulent* and mixing is rapid…In this region the Power Number is essentially constant [5]. A 3-blade retreat impeller, such as the one used in this work, has a Power Number of approximately 0.6 and the N_P vs. Re curve is essentially constant for Re > 10^4 [10] [4]. However, it is evident that the Power Number curves for all three baffling configurations have a definite decreasing trend as the agitation rate is increased for each H/T ratio, as presented in Chapter 4.1 and Appendix A.1. Since this constant curve was not encountered in the collected Power Number data, a separate power dissipation experiment was conducted.

As mentioned earlier, the same retreat blade impeller along with a rushton impeller was used for the supplemental data collection. A rushton impeller was specifically used because it has well known mixing characteristics and a constant N_P vs. Re profile for Re > 10^4 with the corresponding Power Number of approximately 5 for a fully baffled vessel [10] [4]. Three locations are considered for both the impellers, i.e. impeller clearance, C, of 100 mm (C_1), 170 mm (C_2), and 200 mm (C_3).

It can be seen from Figure 4.6, in Chapter 4.2, that the rushton impeller does indeed have a fairly constant N_P vs. Re profile, unlike the profile for the retreat blade impeller. Again, it is noticed that the curve for the retreat blade has a small decreasing trend at each of the impeller clearances considered. It was established in Chapter 2.1 that for a given system geometry the Power Number is dependent on the baffling type, impeller type and geometry, and H/T for Re> 10^4. However, when an

impeller, H/T and baffling configuration is selected, N_P in Equation 2.5 becomes a constant. Although the profile for the rushton conforms to the standard profile, the Power Number is still less than the standard value of 5. This can be attributed to the fact that in an unbaffled tank, a forced vortex zone dominates the vessel flow…and Power Numbers decrease with increasing Reynolds Number [9]. Although, the supplemental experiments were done in a *fully baffled* system, the geometry of the mixing vessel with the torispherical bottom is such that there is an "unbaffled" region bellow the four vertical baffles. Both the rushton and retreat blade impellers are in this "unbaffled" region for an impeller clearance of C_1, "partially baffled" region for C_2 and in a "fully baffled" region for C_3.

These types of baffling environments, for the rushton impeller, does not affect the standard Power Number curve for $Re > 10^4$, but the Power Numbers are less than 5. In fact, this difference in the Power Numbers can be explained. The existence of the "unbaffled" region in the vessel can potentially affect the torque and, hence, the power measurements. For the rushton impeller, this meant a fairly constant N_P vs. Re profile, but lower Power Numbers as seen in Figure 4.6

Additionally, for the retreat blade impeller, this meant a decreasing trend in the N_P vs. Re profile and higher Power Numbers. Following the theory presented in Chapter 2.1, Equation 2.5 becomes a constant for a given H/T, impeller type and baffling configuration. This does not mean that the theory is wrong, but it is not entirely applicable to the system in question because Equation 2.5 does not account for a system with "multiple" baffling configurations. It simply means that presence of the "unbaffled" region in a *fully baffled* system introduces a new kind of system. This new system affects

the power measurements in such a way that the presence of the "unbaffled" region introduces the decreasing trend in the Power Number, but it is small because of the presence of the baffles.

The existence of the "unbaffled" region can also explain the general decreasing trend in the Power Number data, as presented in Chapter 4.1 and Appendix A.1, for the retreat blade impeller as the agitation rate is increased at *each* H/T ratio and baffling configuration. This is especially valid for the fully baffled system and meaningful because the retreat blade impeller clearance is kept at a constant C of 100 mm, where the "unbaffled" region exists.

5.2 Blending Time and Dimensionless Blending Time Discussion

Generally, the results indicate that the blending time is inversely proportional to the agitation rate for the partially and fully baffled systems, but some deviations are present at lower H/T ratios. As the agitation rate is increased, the blending time decreases for all H/T ratios and baffling configurations. This means that the blending time is indeed a function of the fill ratio, agitation rate and baffling configuration as discussed in Chapter 2.2. This dependence is also evident in Figures 4.11-4.13 and Figure 4.17. The blending time for the unbaffled system behaves erratically and has a steep decreasing trend for all of the agitation rates at each H/T ratio. This is probably due to the presence of the vortex at the center of the vessel which increases in size as the agitation rate is increased.

Furthermore, the dimensionless blend time is generally constant in the fully baffled system for the H/T ratio of 0.7 to 1, albeit the presence of minor deviations. Again the theory that the dimensionless blending time is constant for the *baffled system* at *each* H/T ratio is proved to be true. For the range of $0.4 \leq H/T \leq 0.6$, the dimensionless

blend time starts to behave erratically. The same kind of deviation and erratic behavior is also present for the partially baffled system at the respective H/T range. The unbaffled system, on the other hand, does not follow a particular trend for the H/T ratios of 0.3-1. The deviations in both the blending time and dimensionless blending time can be attributed to the presence of the "unbaffled" region in the vessel bottom that becomes dominant for H/T < 0.8. Furthermore, the dependence of both the blending time and dimensionless blending time on the fill ratios and baffling configurations, as evident in Figures 4.14-4.16 and Figure 4.18, can also help explain the irregular behavior.

Blending time experiments, which utilized the colorimetric method, have been previously conducted at an H/T ratio of 1 for all three baffling systems [2]. However, only the 100-200 rpm agitation rates were considered. Nonetheless, the previous data does not compare favorably with the data collected in this work, particularly for the unbaffled and partially baffled systems. For the unbaffled system, a blending time range of 61-248 s was achieved for the 100-200 rpm range in the previous work. However, the blending time for the unbaffled system found in this research work was in the 43-171 s range for 100-200 rpm with 432.33 s for 75 rpm. Similarly, for the partially baffled system, a blend time range of 8-31 s for the 100-200 rpm agitation rates was presented in the previous work, whereas a blend time range of 9-25 s for 100-200 rpm is found in this work. On the other hand, the blend time for the fully baffled system in this work agrees very well with that from the previous research work at each agitation rate between 100 and 200 rpm. The results from the present work indicate a blend time range of 7-17 s for 100-200 rpm which is similar to the 7-14 s blend time range for the same agitation range in the earlier work. The same type of comparison can be made for the dimensionless

blend time between these two works for all three baffling systems. Table 5.1 lists the blend time data from both works and the percent difference.

It is noticed that the blend time and, hence, the dimensionless blend time in both of these works compare favorably at higher agitation rates (i.e. particularly at 150 and 200 rpm) for the fully baffled system. A potential reason is that the flow dynamics at these agitation rates is such that the system is not affected by the presence of the "unbaffled" region in the torispherical bottom section of the mixing vessel. Another reason, applicable to all of the baffling systems, could be that there is a vortex that is present which can affect both the blend time and dimensionless blend time.

Furthermore, there is the difference of the impeller and baffle clearance that needs to be considered. In the previous the work, an impeller clearance, C, of 40 mm was used, whereas 100 mm is used in this work. Additionally, the beavertail baffle and the four baffles (i.e. for the partially and fully baffled systems, respectively) had a baffle clearance of 90.23 mm and 150 mm, respectively. However, this work utilizes a baffle clearance of 170 mm for both the partially and fully baffled systems. Any combination of the above reasons can help explain the lack of conformity of results between the two works for each baffling configuration.

A final note to make is that the author of the previous work used distilled water for all the colorimetric experiments, whereas this work utilized deionized water. This can potentially affect the blending time results. As a matter of fact, the blending time in this work was lower after each repetition of a single experiment at each sampling point. For example, the highest difference of 63% is observed between 2 trials for the *unbaffled* system at an H/T of 0.9. A 40-50% and 45-60% difference between trials is the largest

observed for partially and fully baffled systems, respectively. The magnitude of the differences in the trials decreased considerably for all of the baffling systems as the H/T ratio was decreased, but increased again for the partially and fully baffled systems at low H/T ratios.

Table 5.1 Blending Time Comparison and Percent Difference between Two Studies for Different Baffling Configurations, Agitation Rates, and H/T of 1

	θ_{95} (s)					
N (RPM)	**Unbaffled**	**Unbaffled[2]**	**Partially Baffled**	**Partially Baffled[2]**	**Fully Baffled**	**Fully Baffled[2]**
75	432.33	-	33.82	-	17.18	-
100	161.01	248.23	25.72	31.06	13.56	14.33
125	171.33	123.38	22.76	24.85	10.89	12.37
150	162.14	98.81	18.89	18.98	9.47	9.21
175	43.48	65.72	15.75	13.20	8.73	8.24
200	49.64	67.10	9.82	8.90	7.64	7.27

	% Difference		
	Unbaffled	**Partially Baffled**	**Fully Baffled**
75	-	-	-
100	42.63	18.81	5.52
125	32.54	8.78	12.73
150	48.54	0.48	2.79
175	40.73	17.62	5.77
200	29.91	9.83	4.96

CHAPTER 6

CONCLUSIONS

A number of conclusions can be drawn from the results obtained in this work, as follows:

- Power Number vs. Reynolds Number plots indicates that there exists a decreasing trend in the Power Number for all three baffling configurations and fill ratios.
- Due to the lack of a constant N_P vs. Re profile for the retreat blade impeller in the *fully baffled* system and an H/T of 1 over Re > 10^4, a rushton impeller was used to collect power measurements at varying impeller clearances to set a standard.
- The rushton impeller was found to have a standard N_P vs. Re profile with minor deviations at each of the impeller clearances with a Power Number of less than the standard of 5.
- It is concluded that the presence of the torispherical bottom introduces an "unbaffled" region in the system, even when fully baffled, which affects the power measurements for the retreat blade impeller.
- Furthermore, Power Number results from this work and the data presented in the literature can potentially have large deviations due to the dependence of the Power Number on the type of baffles and baffling configurations, fill ratios, system geometry, impeller Reynolds Number and impeller types and geometry.
- Blending time is found to be inversely proportional to the agitation rate for the partially and fully baffled systems. The same relationship is not entirely applicable to the unbaffled system.
- Dimensionless blending time is found to be fairly constant and linear for the partially and fully baffled systems between fill ratios of 0.7 and 1, albeit small

deviations, while the remaining fill ratios indicate an erratic behavior for both of these systems. The unbaffled system does not follow a specific trend.

- The blending time and dimensionless blending time results indicate that they both are functions of the fill ratio, impeller Reynolds Number and baffling configuration for a given impeller type and system geometry.
- Data, from a previous work on blending time and dimensionless blending time, agrees very well with the results in this work for the fully baffled system with an H/T ratio of 1. However, this level of conformity decreases as the system goes from partially baffled to completely unbaffled.
- It is concluded that the differences in results in the blending time, i.e. between this work and the previous work, can be attributed to several factors including the utilization of different impeller and baffle clearances and the use of deionized water over distilled water.
- Results for both the impeller power dissipation and blending time for all three baffling configurations and fill ratios below 1 cannot be compared due to the lack of information in literature. It is suggested that further experimental work, PIV, or CFD simulations (where applicable) be conducted to check for validity and reproducibility.

APPENDIX A

A.1 Impeller Power Dissipation Results

Table A.1 Agitation Rates, Power Number, and Reynolds Number for the Retreat Blade Impeller for Different Baffling Configurations and H/T of 0.6-0.9

			Power Number, N_P		
H/T	**Agitation Rate, N (RPM)**	**Reynolds Number, Re**	**Unbaffled**	**Partially Baffled**	**Fully Baffled**
0.9	75	51164.25	0.368	0.558	0.823
	100	68219.01	0.316	0.532	0.755
	125	85273.76	0.283	0.517	0.759
	150	102328.51	0.288	0.527	0.750
	175	119383.26	0.272	0.518	0.741
	200	136438.01	0.271	0.516	0.723
0.8	75	51164.25	0.345	0.529	0.800
	100	68219.01	0.295	0.490	0.760
	125	85273.76	0.271	0.474	0.766
	150	102328.51	0.263	0.479	0.753
	175	119383.26	0.254	0.475	0.754
	200	136438.01	0.249	0.470	0.727
0.7	75	51164.25	0.324	0.485	0.815
	100	68219.01	0.277	0.444	0.766
	125	85273.76	0.253	0.428	0.781
	150	102328.51	0.247	0.429	0.780
	175	119383.26	0.243	0.426	0.772
	200	136438.01	0.248	0.438	0.740
0.6	75	51164.25	0.282	0.405	0.784
	100	68219.01	0.238	0.381	0.741
	125	85273.76	0.226	0.382	0.751
	150	102328.51	0.219	0.379	0.753
	175	119383.26	0.212	0.375	0.745
	200	136438.01	0.220	0.373	0.713

Table A.2 Agitation Rates, Power Number, and Reynolds Number for the Retreat Blade Impeller for Different Baffling Configurations and H/T of 0.3-0.5

			Power Number, N_P		
H/T	**Agitation Rate, N (RPM)**	**Reynolds Number, Re**	**Unbaffled**	**Partially Baffled**	**Fully Baffled**
0.5	75	51164.25	0.283	0.380	0.710
	100	68219.01	0.240	0.344	0.663
	125	85273.76	0.220	0.327	0.678
	150	102328.51	0.212	0.324	0.677
	175	119383.26	0.215	0.317	0.667
	200	136438.01	0.227	0.303	0.657
0.4	75	51164.25	0.265	0.300	0.359
	100	68219.01	0.223	0.259	0.336
	125	85273.76	0.197	0.237	0.357
	150	102328.51	0.171	0.214	0.347
	175	119383.26	0.137	0.166	0.317
	200	136438.01	0.122	0.142	0.275
0.3	75	51164.25	0.113	-	-
	100	68219.01	0.079	-	-
	125	85273.76	0.057	-	-
	150	102328.51	0.051	-	-
	175	119383.26	0.047	-	-
	200	136438.01	0.042	-	-

A.2 Blending Time and Dimensional Blending Time Results

Table A.3 Blending Time and Dimensionless Blending Time for Different Baffling Configurations, Agitation Rates, and H/T of 0.8-0.9

		θ_{95} (s)			$\theta_{95}N$		
H/T	**Agitation Rate, N (RPM)**	**Unbaffled**	**Partially Baffled**	**Fully Baffled**	**Unbaffled**	**Partially Baffled**	**Fully Baffled**
0.9	75	182.21	27.19	12.17	227.76	33.99	15.21
	100	158.06	21.26	10.65	263.43	35.43	17.75
	125	130.91	18.62	9.36	272.73	38.79	19.50
	150	101.23	9.70	9.13	253.08	24.25	22.83
	175	57.93	12.65	8.07	168.96	36.90	23.54
	200	44.83	7.84	6.44	149.43	26.13	21.47
0.8	75	160.61	21.86	8.99	200.76	27.33	11.24
	100	65.93	16.58	8.76	109.88	27.63	14.60
	125	105.96	15.31	6.07	220.75	31.90	12.65
	150	74.67	11.70	5.92	186.68	29.25	14.80
	175	29.55	9.96	5.03	86.19	29.05	14.67
	200	22.84	7.01	5.63	76.13	23.37	18.77

Table A.4 Blending Time and Dimensionless Blending Time for Different Baffling Configurations, Agitation Rates, and H/T of 0.3-0.7

		θ_{95} (s)			θ_{95}N		
H/T	**Agitation Rate, N (RPM)**	**Unbaffled**	**Partially Baffled**	**Fully Baffled**	**Unbaffled**	**Partially Baffled**	**Fully Baffled**
0.7	75	115.79	25.48	12.19	144.74	31.85	15.24
	100	75.03	14.28	9.25	125.05	23.80	15.42
	125	45.71	11.95	6.34	95.23	24.90	13.21
	150	24.70	10.02	7.05	61.75	25.05	17.63
	175	20.13	6.72	3.65	58.71	19.60	10.65
	200	17.88	6.65	3.76	59.60	22.17	12.53
0.6	75	80.13	17.72	8.25	100.16	22.15	10.31
	100	52.31	13.13	5.38	87.18	21.88	8.97
	125	54.62	9.17	6.65	113.79	19.10	13.85
	150	18.86	7.31	6.86	47.15	18.28	17.15
	175	15.05	9.57	2.44	43.90	27.91	7.12
	200	6.65	5.41	3.47	22.17	18.03	11.57
0.5	75	31.79	12.12	9.11	39.74	15.15	11.39
	100	25.36	12.45	10.46	42.27	20.75	17.43
	125	27.79	7.93	5.72	57.90	16.52	11.92
	150	11.37	8.55	5.66	28.43	21.38	14.15
	175	21.70	5.99	4.85	63.29	17.47	14.15
	200	12.01	6.44	4.08	40.03	21.47	13.60
0.4	75	12.48	17.56	16.86	15.60	21.95	21.08
	100	9.32	13.51	20.46	15.53	22.52	34.10
	125	13.26	9.45	11.54	27.63	19.69	24.04
	150	18.41	8.15	7.41	46.03	20.38	18.53
	175	6.33	8.22	7.37	18.46	23.98	21.50
	200	9.53	6.32	7.00	31.77	21.07	23.33
0.3	75	13.11	-	-	16.39	-	-
	100	15.14	-	-	25.23	-	-
	125	13.80	-	-	28.75	-	-
	150	13.00	-	-	32.50	-	-
	175	12.25	-	-	35.73	-	-
	200	15.71	-	-	52.37	-	-

A.3 Vortex Formation Data

Table A.5 Vortex Formation at Specific Agitation Rates for Each Baffling Configuration and Fill Ratio

	Vortex Formation		
	Unbaffled	**Partially Baffled**	**Fully Baffled**
H/T	**Agitation Rate, N, (RPM)**		
1	75-100	100-125	200 (variable, randomly located)
0.9	75-100	100-125	200 (variable, randomly located)
0.8	75-100	100-125	175-200 (variable)
0.7	75-100	75-100	125-150
0.6	75-100	75-100	100-125
0.5	75-100	75-100	100-125
0.4	75-100	75-100	75-100
0.3	-	-	-

APPENDIX B

B.1 MATLAB Script for Generating an Image from the Video Input

MATLAB Source Code to Obtain an Image from the Video Input

```
% Script for transforming a video clip into an object and generating an
% image of the object.

clear all
clc
global Size
global Picture
obj = VideoReader('filename'); % Transforms a video clip into
% an object.
images = read(obj, [1,Inf]); % Reads the whole object and is named 'images'.
Size = size(images); % The size of 'images '.
Picture = images(:,:,:,1); % The first frame of 'images' is named as 'Picture'.
image(Picture) % An image of 'Picture' is created.
```

B.2 MATLAB Script to Extract the Green Component of the Light Intensity from Individual Sampling Locations

MATLAB Script to Extract the Green Component of the Light Intensity from Individual Sampling Locations

```
% This script generates the color intensity for the Green component which
% will help determine the mixing time.

global Size
global Picture

Video = []; % Corresponds to all the Frames of interest
FPS = 29; % Frames per second of video clip

% Locations containing the points of each image.
Locations = [Point_1.Position;Point_2.Position;Point_3.Position;...
Point_4.Position;Point_5.Position;Point_6.Position;Point_7.Position;...
Point_8.Position;Point_9.Position;Point_10.Position;Point_11.Position;];

% The following code is used to analyze the whole video clip for the Green
% component at all the selected points.
for i = 1:Size(4)
   Picture = images(:,:,:,i);
   Frame = []; % Corresponds to each image
% The loop below is for analyzing all the points of interest in each frame.
for x = 1:11
   Green = Picture(Locations(x,2), Locations(x,1), 2);
   Frame = [Frame; Green];
end
Video = [Video Frame];
end

% Time definition.
Time(1) = 0;
for i = 2:Size(4)
   Time(i) = (i-1)/FPS;
end
```

REFERENCES

1. Cabaret, F., Bonnot, S., Fradette, L., Tanguy, P. A. (2007). *Mixing Time Analysis Using Colorimetric Methods and Image Processing.* Industrial & Engineering Chemistry Research, **46**, 5032-5042.

2. Chomcharn, N. (2009). *Experimental Investigation of Mixing Time in a Stirred, Torispherical —Bottomed Tank Equipped with a Retreat-Blade Impeller.* M.Sc. Thesis, Otto H. York Department of Chemical, Biological and Pharmaceutical Engineering, New Jersey Institute of Technology, Newark, NJ.

3. Dickey, D. S., Bittorf, K. J., Ramsey, C. J., Johnson, K. E. (2004). *Understand Flow Patterns in Glass-lined Reactors*. Chemical Engineering Progress, 21-25.

4. Dickey, D. S., Patterson, G. K. (2008). *Find Mixing Success Through Failures Part 1*. Chemical Engineering Progress, 40-47.

5. Harnby, N., Edwards,M.F., Nienow, A.W. (1985). *Mixing in the Process Industries Second Edition*. Oxford, UK: Reed Educational and Professional Publishing Ltd.

6. Holland, F. A., Chapman, F. S. (1966). *Liquid Mixing and Processing in Stirred Tanks*. New York, N.Y.: Reinhold Publishing Corporation.

7. Motamedvaziri, S. (2012). *Single and Multiphase Mixing in Partially Filled Stirred Vessels*. Ph.D. Dissertation, New Jersey Institute of Technology, Newark, NJ.

8. Myers, K. J., Reeder M.F., Fasano, J. B. (2002). *Optimize Mixing by Using the Proper Baffles.* Chemical Engineering Progress, **98**(2), 42-47.

9. Oldshue, J. Y. (1983). *Fluid Mixing Technology*. New York, N.Y.: Chemical Engineering McGraw-Hill Publications Co.

10. Paul, E. L., Atiemo-Obeng, V. A., Kresta, S. M. (2004). *Handbook of Industrial Mixing: Science and Practice*. Hoboken, N.J.: John Wiley & Sons, Inc.

11. Post, T. (2010). *Understand the Real World of Mixing*. Chemical Engineering Progress, 25-32.